Simulation Tools for
Hybrid Electric Vehicle Architecture Simulations

Undergraduate Honors Thesis

Presented in Partial Fulfillment of the Requirements for

Graduation with Distinction at

The Ohio State University

By

Arjun Khanna

* * * * *

The Ohio State University

2014

Defense Committee:

Dr. Giorgio Rizzoni

Dr. Shawn Midlam-Mohler

ABSTRACT

Increasingly stringent regulations on emissions require automobile manufacturers to find new ways to reduce the emissions produced by their vehicles. If current trends provide for an indication of where the automotive industry is headed, hybrid electric vehicles (HEVs) and electric vehicles (EVs) will become very prevalent in the market in coming years. These technologies are all relatively new and still need much development before they can hold a significant place in the automotive market. It is for this reason that companies are investing heavily in training the next generation of engineers to work on this problem. EcoCAR 3, a four year long Advanced Vehicle Technology Competition (AVTC), is one way companies are pursuing this.

EcoCAR 3 challenges the engineering students to modify a stock Chevrolet Camaro, donated by GM, to reduce the vehicle's energy consumption and tailpipe emissions, while maintaining standard vehicle performance. Due to the presence of multiple components in a HEV (engine, battery-pack and at least one electric machine), the complexity of optimizing the operation of the vehicle's powertrain components significantly increases in comparison to a conventional vehicle. One of the topics that EcoCAR 3 series stresses during year 1 is architecture selection for the Chevrolet Camaro, which involves the team to select a vehicle architecture that meets the goals of both the competition and the team. Increasing demand for HEV designs require automated

modeling and simulation tools to construct a design space search. Composability and scalability are highly desirable in these simulators to provide design candidates.

The work described in this project focuses towards the tools developed and the validation done for these tools. These tools were developed for the EcoCAR 3 team of the Ohio State Universiy, which would provide assistance in generating different size engine fuel consumption maps and different size electric machine efficiency maps quickly. The maps generated by these tools can then be utilized to test how varying engine and electric machine sizes can affect the overall performance of the vehicle with different architectures.

ACKNOWLEDGMENTS

I would like to thank Dr. Giorgio Rizzoni for the chance to participate in this undergraduate research project. I would especially like to thank Dr. Shawn Midlam-Mohler, for all the guidance he has given me during this research project. I would like to thank the entire EcoCAR team, especially Katherine Bovee and Matt Yard for introducing me and helping me learn about Hybrid Electric Vehicles.

TABLE OF CONTENTS

Page

LIST OF FIGURES

LIST OF TABLES

CHAPTER 1: INTRODUCTION

1.1 Motivation

Today, the increasing number of vehicles worldwide is causing a significant negative impact on air quality and human health [1]. Emissions standards set by the U.S. Environmental Protection Agency (EPA) are getting more stringent in addition to the rising petroleum prices [2]. Because of all these factors, the rate of vehicle technology change in the automotive industry is increasing and moving towards a low-carbon future [3], meaning less emissions pertaining to carbon monoxide (CO), nitrogen oxides (NOx) and greenhouse gases (GHG).

If current trends provide for an indication of where the automotive industry is headed, hybrid electric vehicles (HEVs) and electric vehicles (EVs) will become very prevalent in the market in the coming years [3]. HEVs consist of powertrains that combine more than one form of energy. For example, the Chevrolet Volt is an HEV that combines a conventional gasoline powered engine with electrical power generation provided from a battery pack. EVs consist of a powertrain powered solely by electricity, usually coming from a battery pack.

These technologies are all relatively new and still need much development before they can hold a significant place in the automotive market. It is for this reason that companies are investing heavily in training the next generation of engineers to work on this problem. EcoCAR 3, an Advanced Vehicle Technology Competition (AVTC), is one

way companies are pursuing this.

1.2 EcoCAR 3

The Ohio State University is taking part in a four year long Advanced Vehicle Technology Competition (AVTC), EcoCAR 3. This competition is headline sponsored by The U.S. Department of Energy and General Motors (GM) the competition is managed by Argonne National Laboratory. The purpose of this competition is for collegiate student teams to reduce the environmental impact of a vehicle by minimizing fuel consumption and reducing its emissions, while maintaining the vehicle's original performance and consumer acceptability. The team will be provided with a stock Chevrolet Camaro, donated by GM. Each team's task will be to design, build, and optimize a new powertrain for their vehicle, resulting in a fully functioning prototype vehicle by the end of the fourth year. The prototype vehicles created by each team will be evaluated over a wide range of metrics that include the vehicle's fuel economy, its emissions, drivability, acceleration, consumer acceptability, and braking.

The competition is broken up into four years and there is a final competition at the end of each year. The EcoCAR 3 competition started in the fall of 2014 and is currently in its first year. In the first year of the EcoCAR 3 competition series stresses the application of the Vehicle Development Process, math-based modeling tools, architecture selection, communications, and project management.

1.3 Project Objective

One of the topics that EcoCAR 3 series stresses on during year 1 is the architecture selection for the Chevrolet Camaro, which involves the team to select a vehicle architecture that meets the goals of both the competition and the team. To select the best architecture the team needs to have a solid understanding of the strengths and weaknesses of various powertrains. To understand these strengths and weaknesses, team needs to evaluate multiple powertrain components and subsystems as part of a total vehicle system, and finally choose or reject the specific components (e.g., engines, motors, batteries, transmissions, subsystems) for their proposed vehicle.

The entire process of evaluating each component that best fits the needs for the team and competition is tedious. This project develops tools for the EcoCAR 3 team, which would provide assistance in generating different size engine fuel consumption maps and different size electric machine efficiency maps quickly. The maps generated by these tools can then be utilized to test how varying engine and electric machine sizes can affect the overall performance of the vehicle. This would allow the EcoCAR 3 team to make an informed decision on what size engine and electric machine could be used in different architectures. This would eventually help the team select the architecture that best fits the competition and the consumer needs which eventually gives the team a direction for the rest of the competition.

CHAPTER 2: LITERATURE REVIEW

2.1 Hybrid Electric Vehicle

There has been much research and advancement in recent years in the area of electrification of vehicles. The three major kinds of electrified vehicles that are being commercially produced are Electric Vehicles (EV), Hybrid Electric Vehicles (HEV) and Plug-in Hybrid Electric Vehicle (PHEV) [4]. Each of the three kinds of electrified vehicle have their respective components and their pros and cons, which are discussed in this section.

Electric Vehicles also known as Battery Electric Vehicles (BEV) consists of a high voltage battery pack and single or multiple motors to propel the vehicle. The highly efficient electric machines that take the electricity from the battery pack and convert it into mechanical power contribute to the overall higher efficiency of EVs than a conventional ICE vehicle [4], [5]. The EVs have zero “Pump to Wheel” tail-pipe emissions because the vehicle runs one hundred percent on electricity. Regenerative braking is an energy recovery mechanism that can be implemented in an EV. This mechanism slows a vehicle down by converting the kinetic energy of the vehicle into electricity, which is stored in the battery pack until needed. This allows EVs to recover energy that would normally be lost in the braking process. Some of the concerns regarding an EV include the high purchase cost of the components, and the life cycle of a high voltage battery pack before it needs to be replaced. One of the disadvantages is the range for entirely electric vehicle which is typically only 100 miles before it needs to be recharged due to the lower charge density of

the battery [4]. The issue of charging also brings up the issue of city infrastructure. To allow for an EV to travel long distances, city infrastructure all over the nation needs to change to include charging stations to make it possible for electric vehicle to recharge its batteries just like conventional cars re-fuel today. Despite the disadvantages, the advancement of technology in the future could make the use of electric vehicles a viable and a beneficial choice for the everyday consumer and the environment.

Hybrid electric vehicles (HEVs) were developed to overcome the limitations of ICE vehicles and EVs [6]. HEVs are a subset of hybrid vehicles, which utilizes both the liquid fuel (gasoline, diesel, E85 etc.) as well as electricity to provide power to the wheels. Some of the major components that go into the making of an HEV power-train are: internal combustion engine, a battery pack and at least one electric machine [4]. The previously mentioned components are also illustrated in Figure 1. Having two propulsion systems within the same vehicle provides some advantages to HEVs over a conventional vehicle. One of the advantages in a HEV is that a downsized engine can be used with the high voltage battery pack and a motor to propel the vehicle. This provides a HEV the ability to have high performance while providing better fuel economy and reduced emissions. Due to the internal combustion engine in HEVs, it allows the vehicle to have the same travelling range as a conventional vehicle [4]. Just like EVs the HEVs get to utilize the regenerative braking. Although there are a lot of advantages of using a HEV, there are some shortcomings as well. One of the major drawbacks of HEVs currently is the purchase price for consumers due to the added components making them out of reach for consumers even though HEVs provide better fuel economy. Another disadvantage of HEVs over EVs is the

lack of all-electric mode in the vehicle. The option of a Plug-in Hybrid Electric Vehicle (PHEV) can solve the problem of all electric range of a HEV.

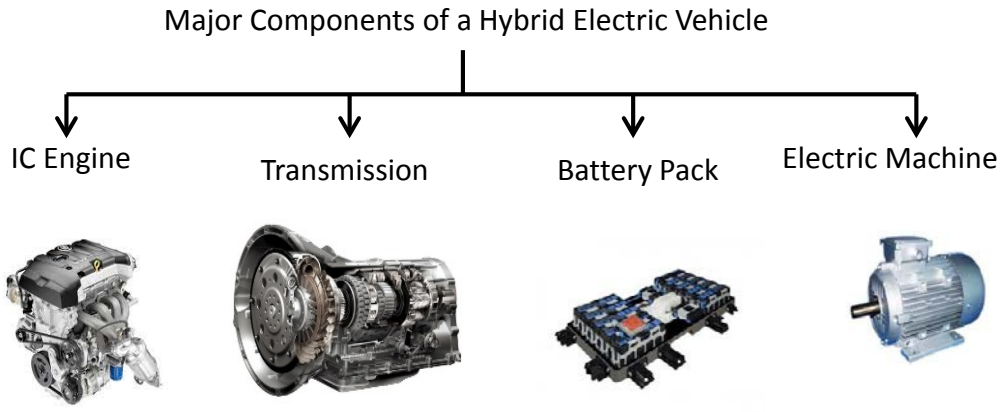

Figure 1: Major Components of a Hybrid Electric Vehicle

A Plug-in Hybrid Electric Vehicle has been defined by SAE [7] as: "A hybrid vehicle with the ability to store and use off-board electrical energy in the RESS (rechargeable energy storage system)." These systems are in effect an incremental improvement over the HEV with the addition of a large battery with greater energy storage capability, a charger, and modified controls for battery energy management and utilization. The better fuel economy, longer travelling range and better performance are some of the positive elements concerning PHEVs which can run on 100% electric mode for short distances. Like both the EVs and HEVs, PHEVs also have a high purchase price [8].

Various combinations of architectures and sizes of components can influence the performance attributes of an HEV significantly. Some of the major HEV components,

architectures and techniques used to scale the internal combustion engines and electric machines are described in the following sections.

2.2 HEV Architectures

The energy flow through the components of a Hybrid Electric Vehicle can be arranged and configured in various ways that define the architecture of the vehicle. This section of the thesis reviews the different possible HEV architectures, their respective operating modes, and their pros and cons.

2.2.1 Series

In series HEV architecture, an engine is coupled with an electric machine, which works as a generator to convert the energy produced by the engine into electricity which is used to charge the battery pack. The battery provides power to a second electric machine that converts the electricity to mechanical power which in turn propels the vehicle [9]. Figure 2 shows a model of plug-in series hybrid electric drivetrain. There are six possible different operation modes in a plug-in series HEV:

1) Battery alone mode: engine is off and the vehicle is powered by the battery only;

2) Engine alone mode: power from ICE only;

3) Combined mode: both ICE set and battery provides power to the traction motor;

4) Power split mode: ICE/G power split to drive the vehicle and charge the battery;

5) Stationary charging mode;

6) Regenerative braking mode [5].

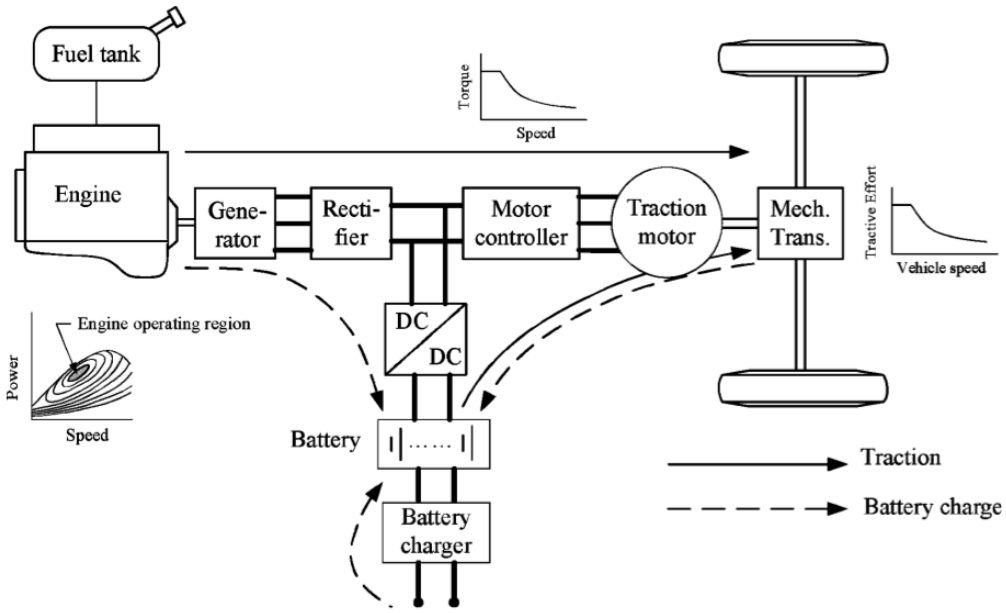

Figure 2: Plug-in Series Hybrid Electric Vehicle [9]

Decoupling engine from the wheels provide some advantages to the series HEV architecture. The first advantage being that the flexibility to place the ICE anywhere in the car [6]. Also, because the engine is not directly connected to the wheels in the series HEV, the vehicle has the option to run the internal combustion engine in its optimal operating range the entire time which allows the HEV to have a greater engine efficiency. A multi-gear transmission in this architecture is unnecessary because of favorable torque-speed characteristics of the electric motor. The controls and packaging are simpler because of the

simpler drive train. Only electrical cables connect the batteries, the generator and the traction motor.

In addition to the advantages of a series HEV architecture, there are some disadvantages as well. Perhaps the greatest disadvantage is the lower efficiency of the series hybrid electric vehicle outside of its optimal range. The lower efficiency is caused by the need for three propulsion devices: the ICE, the generator, and the electric motor. Similar to EVs, extra precautions come in to play when the vehicle needs to make lengthy trips versus short commutes to work or the supermarket. The series HEV will need to have the traction motor sized to provide maximum sustained power since it is the only traction source, which will make the overall vehicle's price go up. For shorter trips this would not be the case but for the vehicle to travel long distances the consumer may have a high out of pocket cost [6]. Additionally the series HEV is disadvantaged because it requires two electric machines which means twice the energy conversions causing twice the energy loss. Also the additional motor means more additional weight of the vehicle which affects the overall performance, fuel consumptions and emissions of the vehicle [9].

2.2.2 Parallel

Both the engine and the electric machine are capable of propelling the vehicle at the same time in a parallel HEV architecture. As shown in Figure 3, a plug-in parallel hybrid architecture consists of a battery, an engine and an electric machine. The electric machine and the engine are mechanically coupled together. The mechanical coupling could be one of the following: a gearbox, a pulley-belt unit or a sprocket chain unit or even a

single axle [9]. Figure 4 shows the schematics of previously mentioned possible mechanical couplings in a parallel hybrid electric drive train.

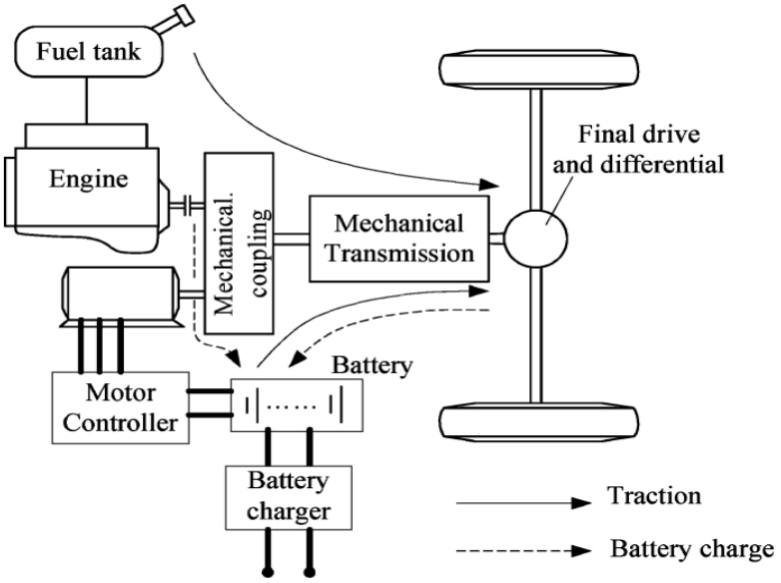

Figure 3: Plug-in Parallel Hybrid Electric Vehicle Architecture [9]

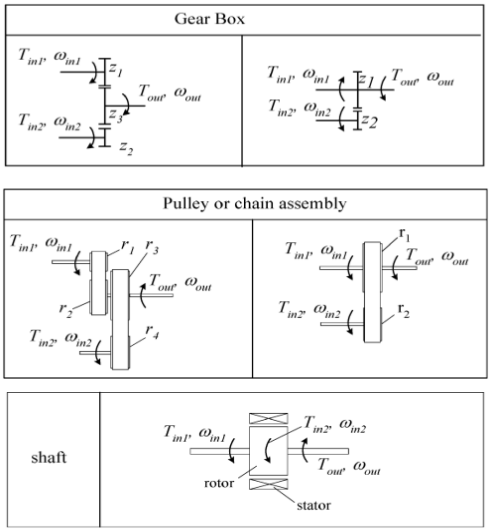

Figure 4: Commonly used Mechanical Torque Couplings [9]

The following are the possible different operation modes of parallel hybrid:

1) Motor alone mode: engine is off, vehicle is powered by the motor only;

2) Engine alone mode: vehicle is propelled by the engine only;

3) Combined mode: both ICE and motor provides power to the drive the vehicle;

4) Power split mode: ICE power is split to drive the vehicle and charge the battery (motor becomes generator);

5) Stationary charging mode;

6) Regenerative braking mode (include hybrid braking mode) [5].

One advantage of the parallel HEV architecture is that it is more efficient than the series architecture because it only requires the internal combustion engine and the electric machine, both of which are directly connected to the wheels. This results in decreased energy loss [4]. Another advantage of the parallel architecture is the compact size due to the reduced number of components as compared to a series HEV [6]. Also, a generator is usually not needed with this configuration and a smaller traction motor can be used [9].

While there are advantages there are a few disadvantages as well. The structure and control of parallel vehicles is complex and due to the mechanical coupling between the driven wheels and the engine, it is difficult for the vehicle to perform in a narrow optimal region in comparison to series HEV [9]. Since the optimal region is not often achievable these vehicles will often employ the use of a clutch for operation [6].

2.2.3 Multi-mode (Power Split)

A multi-mode hybrid vehicle encompasses the features of both the parallel and the series HEV architectures. One ICE and two electric machines in conjunction with different configurations of planetary gear-set or clutches gives the vehicle the extra degree of freedom of switching modes between series and parallel modes.

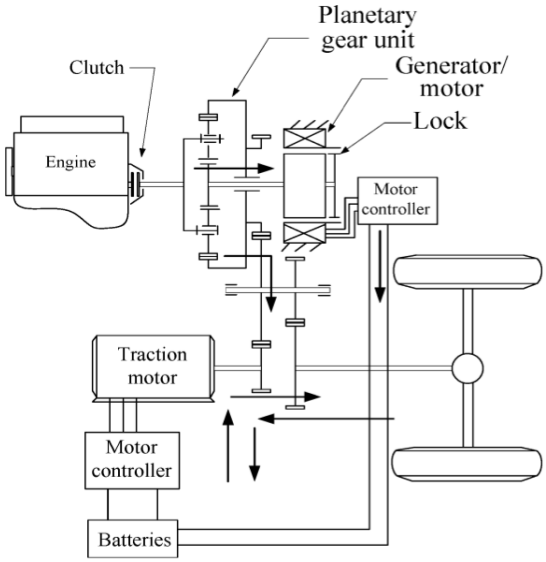

Figure 5: Series-Parallel Hybrid Architecture using a Planetary Gear Unit [9]

Figure 5 explains an example of Toyota Prius' series-parallel architecture. This particular series-parallel hybrid architecture consists of an engine, a generator/motor, a traction motor and a planetary gearbox. Series mode is achieved by using the planetary gear to decouple the engine speed from the wheel speed. The decoupling of the engine from the wheels is done by adjusting the speed of the generator/motor, thus allowing the engine to operate at its most efficient operating points at all times. Additionally, the architecture

is able to operate in a parallel mode by locking the stator and rotor of the generator/motor together and de-energizing it. When stator and rotor of the generator/motor are locked in place, the planetary gear unit becomes a simple gearbox with a single fixed gear ratio, thus allowing the vehicle to operate in parallel mode [9].

The multi-mode configuration combines the best qualities of both series and parallel architectures so that the vehicle will be operating efficiently and deliver high performance [4]. Figure 6 from the United States Department of Energy and the Alternative Fuels Data Center, outlines the overall sales of HEV's in the U.S. market. From Figure 6, it is clear that the Toyota Prius has a commanding market share for HEVs in the United States. What sets the Prius apart from the competition is its advanced vehicle architecture, which is a multi-mode as expressed in Figure 5. The multi-mode HEV architecture is proven to be dominant, so it is a safe assumption to make that a multi-mode HEV is a good balance between cost, complexity, and performance.

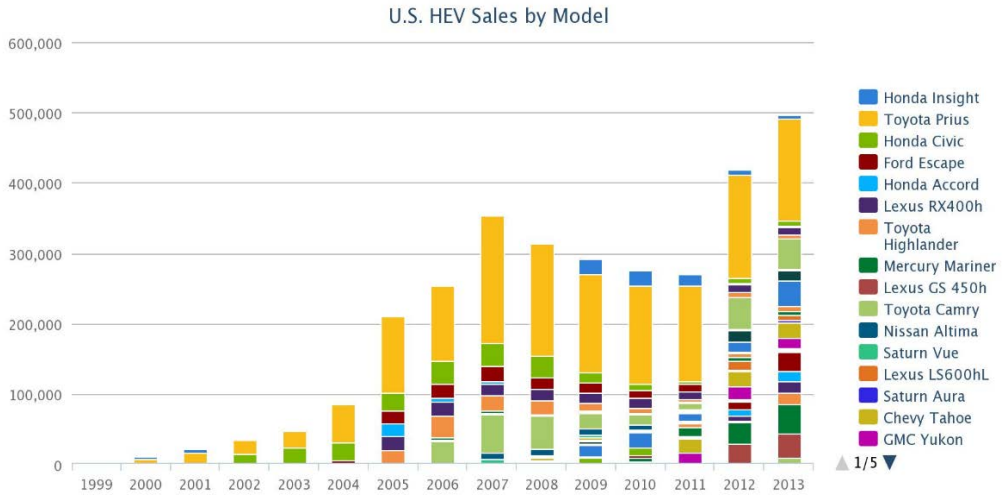

Figure 6: HEV Sales in the United States [10]

2.3 Energy Converters

Energy converters are the components in a HEV that are responsible for energy conversions between energy domains (chemical to mechanical, electrical to mechanical *etc.*) [11]. As represented in Figure 7 and mentioned before HEV's consist of two powertrains and hence two energy converters: engine and electric machine.

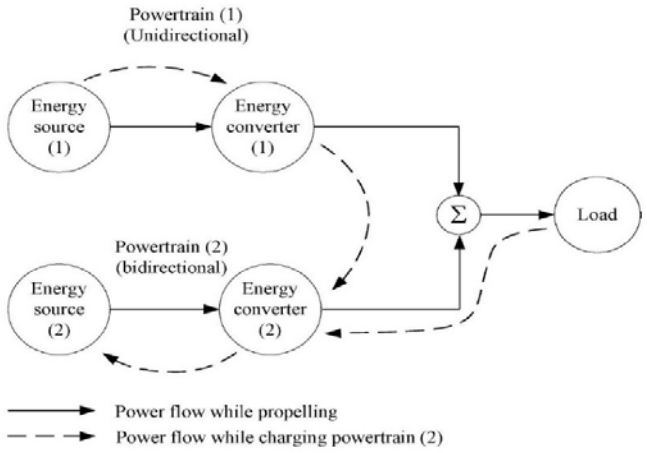

Figure 7: Illustration of Power Flow in a HEV [9]

This section introduces different types of the energy converters, their different performance characteristics due to the differences in the technologies and also mentions the advantages and disadvantages pertaining to the different types of energy converters. This section of the thesis stresses on different technologies and performance aspects because the tools developed for this project are sensitive to these differences.

2.3.1 Internal Combustion Engines

An internal combustion engine is an energy converter that transforms chemical energy into mechanical energy with a certain efficiency. In an Internal combustion engines (ICEs), as opposed to external combustion engines, the energy source is a combustible mixture, and the combustion products is the working fluid. In external combustion engines, the combustion products is used to heat a second fluid that acts as the working fluid [12]. There are many different types of ICEs and performance of these different types of ICE depends majorly on the fuel type used by the engine (Gasoline, E85, Diesel, *etc.*), technology used by the engine (turbo/super-charged, GDI, *etc.*) and the overall size of the engine.

Gasoline engines, approximated by an Otto engines, mix the air and the fuel in the intake system prior to the entry of the engine cylinders using either a carburetor or a fuel injection system. In a diesel engine, the air alone enters the cylinder; without getting mixed with the diesel fuel. The diesel fuel is injected directly into the engine cylinder just before the combustion process is required to start. In the case of spark ignition (SI) engines, the compression ratio of the cylinder is in the range of 9 to 13 and is limited by octane rating of the fuel. In compression ignition (CI) (diesel) engines, the compression ratio for air is 12 to 24. The high compression ratio of air creates high temperatures which ensures the diesel fuel can self-ignite [12]. In the case of CI engines, the value of compression ratio is higher; according to Equation (2.1) CI engines have the potential to achieve higher fuel conversion efficiency while in the case of SI engines the lower

compression ratio reduces their potential to achieve higher efficiency [12]. Dedicated E85 engines, like CI engines benefit from a higher compression ratio as well, increasing their potential to achieve a higher efficiency. This is because E85 has a relatively high octane number making it more tolerant of high compression ratios.

$$\eta_f = 1 - \frac{1}{r_c^{\gamma-1}} \tag{2.1}$$

Performance of an ICE also depends on the technology used in the engine: naturally aspirated (admitting atmospheric air), supercharged (admitting pre-compressed fresh mixture), and turbocharged (admitting fresh mixture compressed in a compressor driven by an exhaust turbine). These technologies have their respective pros and cons which are further described in this section.

A supercharger is an air compressor that increases the pressure or density of air supplied to an ICE, in turn increasing the volumetric efficiency of the engine [12]. Defines volumetric efficiency as the parameter, which is used to measure the effectiveness of an engines induction process. Power for the supercharger in an ICE is usually provided by mechanically coupling the engine's crankshaft to the supercharger by means of a belt, gear, shaft, or chain. A supercharged engine provides excellent low-end torque capabilities and very good response [13]. However, there are some drawbacks associated with supercharging an engine. Due to the mechanical coupling, the engine has to burn extra fuel to provide power to drive the supercharger. The parasitic losses of a supercharger can negate some of the fuel savings of downsizing an engine. Even though, the parasitic losses

of the supercharger can be quite significant at high engine speeds, the indicated mean effective pressure (IMEP) is higher than the IMEP for a naturally aspirated (NA) or turbocharged (TC) engine with the same power output [13].

When power in a supercharger is provided by a turbine powered by exhaust gas of the engine, a supercharger is known as a turbocharger. Turbo charging counteracts the power lost from downsizing without the parasitic losses associated with supercharging. A turbocharged engine also runs at significantly higher BMEP levels than a naturally aspirated engine. The upper limit of BMEP levels that can be expected from a naturally aspirated engine is ~ 13.5 bar, whereas a turbocharged engine can produce BMEP levels in excess of 20 bar [14]. By using a small displacement engine with a turbocharger, the smaller engine works harder (higher in cylinder load) which results in lower pumping losses as the throttle has to be further open [14]. Boosting an engine via turbocharger has its own deficits. Turbocharged systems typically have a delay in response as compared to a supercharged system or naturally aspirated systems [13]. The back pressure increase associated with turbocharging results in an increase in pumping losses and the need to run with lower overlap at higher speed to avoid insufficient exhaust gas scavenging. The turbo also acts as a heat sink, which can slow the catalyst heating and catalyst light-off after start, thus hurting emission reduction strategies [13]. Turbo charger manufacturers are aware of these issues and designs are being validated that address these concerns. A comparison between boosted engines and naturally aspirated engine done by [14] is used to highlight these differences.

Figure 8 compares the brake specific fuel consumption of the DI Boost engine and the LS6 engine at the same torque points at 2000 rpm [14]. Brake specific fuel consumption (BSFC) is the fuel flow rate per unit power output, it is a measure of how efficiently an engine is using the fuel to produce power. Low values of BSFC are desirable [12]. The advantage of boosting in terms of fuel consumption at typical road load conditions can be seen in Figure 8.

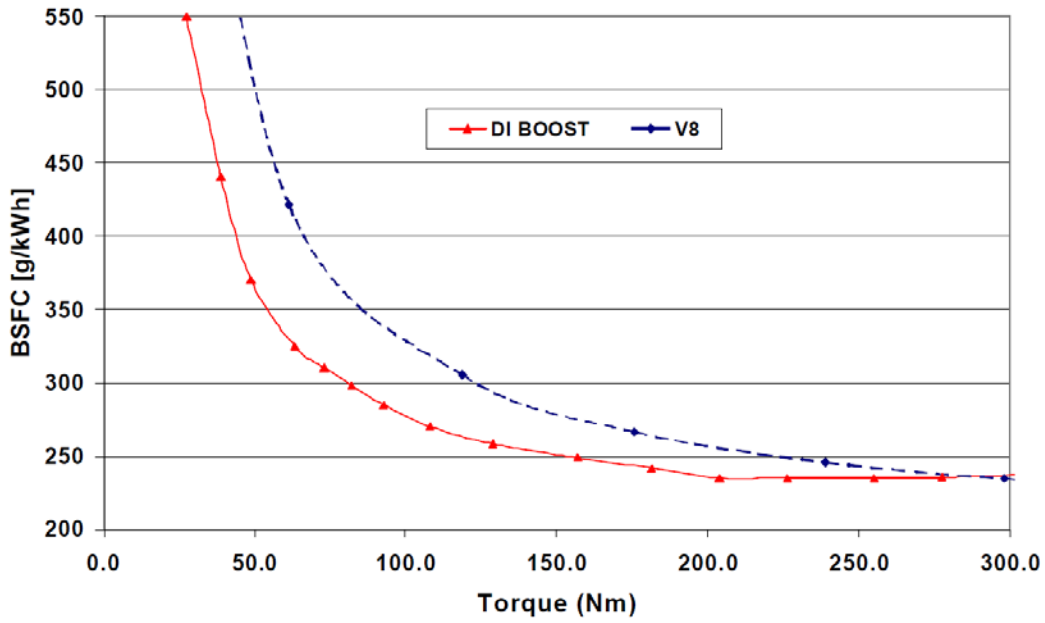

Figure 8: Fuel Consumption at 2000 rpm [14]

It is also proven that in most cases a boosted downsized engine can replace a larger conventional naturally aspirated engine and achieve equivalent power and torque [14]. This fact can be confirmed by looking at Figure 9.

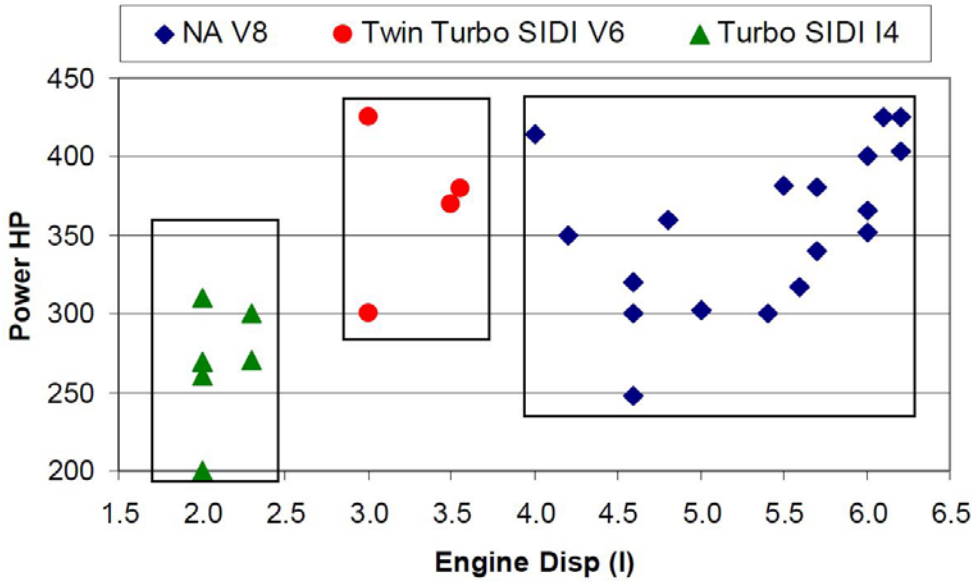

(a)

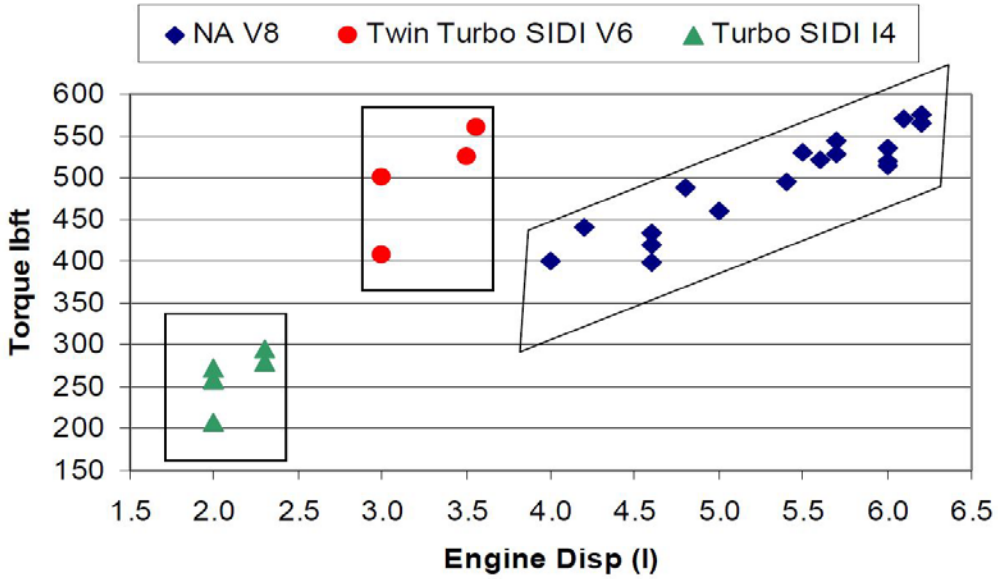

(b)

Figure 9: Comparison of Naturally Aspirated and Turbocharged Downsized Engines (a)Power (HP) (b) Torque (lb-ft) [14]

2.3.2 Electric Machines

One of the major energy converters used in an HEV, other than the engine, is the electric motor [15]. Electric motors convert electricity to mechanical energy and can also act as generators and convert mechanical energy to electrical energy. Some of the EMs require alternating current (AC) to operate, which is provided to the EM by an inverter. An Inverter, is an electronic device or circuitry that changes direct current (DC) from the battery pack to alternating current (AC). The conversion of the power from the battery pack to mechanical and vice-versa depends of the performance of the system that includes the motor and the inverter. The aspect of the EMs to convert energy 2-ways aspect, is especially helpful in a parallel architecture as one component of the vehicle solves two purposes, *i.e.* convert the mechanical energy from the engine to electricity to charge the battery, and also convert the electricity from the battery pack into mechanical energy in order to power the wheels. This ultimately helps in reducing the overall weight of the vehicle. A major advantage of the electric motor in hybrid electric drive is that torque generation is very quick and accurate [16]. This section of the thesis discusses the major kinds of electric machines used in HEVs and their typical performance characteristics.

There are four basic types of motors that can be used in an EV or a HEV: direct-current motor (DC), induction motor (IM), brushless permanent-magnet motor (PM) and switched reluctance motor (SRM).Figure 10 illustrates the cross-sections of the previously mentioned motor types [15].

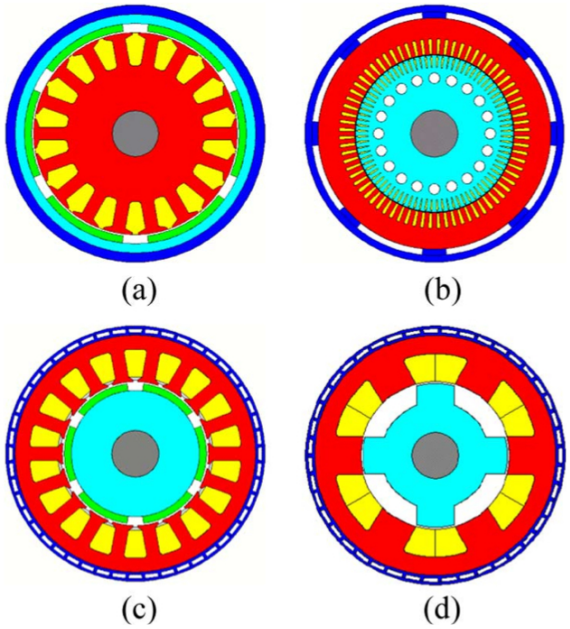

Figure 10: Industrial and Traction Motors' Cross-Section (a) DC Motor (b) IM (c) PM Brushless Motor (d) SRM [15]

Figure 11 shows a standard operational characteristic of how torque varies with respect to speed in any electric motor. Constant torque (or force) region and constant power region are the two major regions that this typical characteristic curve can be distributed into. Within the constant torque region the electric motor provides its constant rated torque up to its base speed. At the base speed the motor reaches its rated power limit. The operation beyond the base speed is called constant power region. In this region the motor provides rated power up to its maximum speed. This is obtained by reducing the field flux of the motor and, therefore, is also known as the 'field- weakening region' [17].

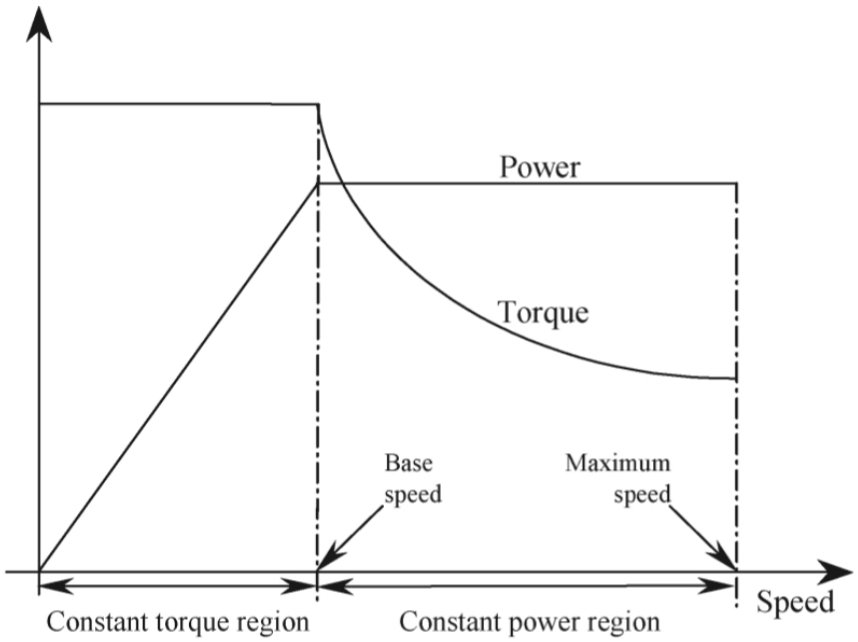

Figure 11: Typical Motor Torque vs. Speed Characteristic [15]

According to exhaustive research done by [15] it has been observed that investigations on the SRMs, IMs, and PM motors are increasing while those on DC motors are decreasing. DC motors work on the principle of magnets; like poles repel and unlike poles attract. The brushed DC electric motor generally consists of windings in the rotor and permanent magnets in the stator. DC motors generate torque directly from the DC power supplied to the motor by using internal commutation, stationary magnets, and the rotating electrical magnets. One advantage of using a DC motor in HEVs are the simple controls associated with the machine [15]. Some of the disadvantages to DC motors include bulky construction, low efficiency, low reliability, and the mechanical commutator (brush) which increases the maintenance cost on these machines [15]. All the previously mentioned disadvantages make it hard to use DC motors in HEVs.

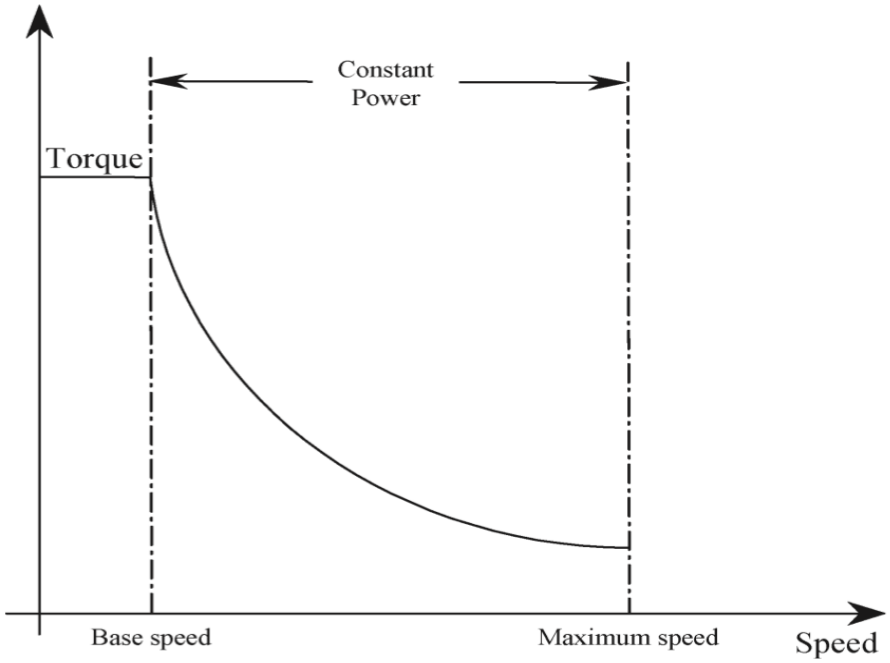

Figure 12: Typical Switched Reluctance Motor Torque vs. Speed Characteristic [15]

Switched reluctance motor is a type of stepper motor and unlike DC motor, the power in an SRM is delivered to the windings in the stator rather than the rotor. The direct current in a SRM generally switches turns in the stators windings. The rotor in a SRM is made of permanent magnets. Because the rotor is out of line with the magnetic field of the stator, a torque is produced to minimize the air gap and makes the magnetic field symmetrical [16]. Figure 12 illustrates the typical SRM torque vs. speed characteristic. From Figure 12 it can be seen that SRMs have a rather long constant power region apt for HEV application. Some of the advantages that relate to these motors include: simple and rugged construction, fault-tolerant operation, simple control, and as previously mentioned SRMs have an outstanding torque-speed characteristic. Other than these advantages acoustic noise generation, torque ripple, special converter topology, and excessive bus

current ripple are some of the disadvantages associated with SRMs. Acceptable solutions to the above disadvantages are needed to achieve a viable SRM-based HEV. Nevertheless, SRM is a solution that is actually envisaged for HEV applications [15].

Induction Motors, unlike DC and SR motors, run on alternating current (AC). The electric current in an IM is supplied to the stator and further electricity is inducted in the rotor by magnetic induction rather than direct electric connection. Figure 13 illustrates a typical induction motor torque-speed curve, which is slightly different than the typical electric motor curve. The curve consists of an additional "high-speed" region, which begins at the motors critical speed beyond which if the motor is operated at maximum current the motor will stall. The critical speed of an IM is typically two times the synchronous base speed where the motor reaches its breakdown torque. The presence of a breakdown torque limits an IM's extended constant-power operation [15].

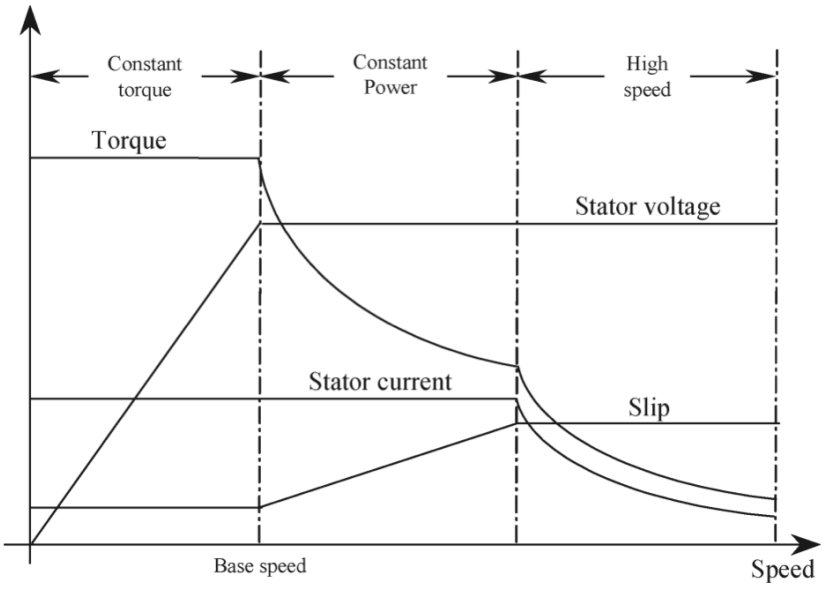

Figure 13: Typical Induction Motor Torque vs. Speed Characteristic [15]

Advantages pertaining to induction motors are: high reliability, ruggedness, low maintenance, low cost, and ability to operate in hostile environment. These qualities make IMs one of the most accepted candidates for application in HEVs [15]. Other than the advantages, some of the disadvantages for IMs are: high energy loss, low efficiency, low power factor, and low inverter-usage factor, which is more serious for the high speed, large power motor. Also, IMs efficiency is inherently lower than that of permanent magnet motors, due to the absence of rotor winding and rotor copper losses [15]. To improve the IM drive's efficiency, a new generation of control techniques have been proposed. Also, to extend the constant-power region, multi-phase pole changing IM drives have been suggested [15].

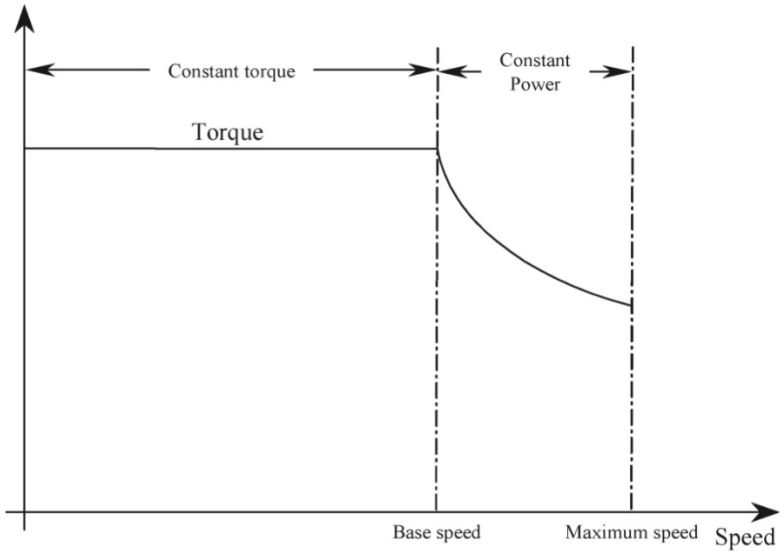

Figure 14: Typical Permanent Magnet Brushless Motor Torque vs. Speed Characteristic [15]

Permanent magnet (PM) brushless motors utilize alternating current just like induction motors. It is called permanent magnet brushless because the armature has no

brushes connected to it and the rotor consists of a permanent magnet. Magnetic field is generated by the stator, which takes alternative supply from a DC source. The rotor moves because of the interaction with the magnetic field generated by the stator [16]. Figure 14 illustrates the typical PM brushless motor's torque-speed performance characteristics. From Figure 14 it is evident that PM brushless motors have a relatively shorter constant-power region as compared to the other motors discussed earlier in this section. The shorter constant-power region of these motors is due to their rather limited field weakening capability, resulting from the presence of the PM Field (the fixed PM limit their extended speed range). Another disadvantage is that it is costlier due to the presence of permanent magnet [17] ,[16].

Compared to IM's, PM brushless motors are currently better contenders for use in HEVs. This is due to their following advantages: high power density, higher efficiency, and the ability to dissipate heat to the surroundings with a higher efficiency. The PM brushless motor is thus most suited for HEVs [15].

2.4 Scalable Approach to HEV modeling

Increasing demand for HEV designs require automated modeling and simulation tools to construct a design space search. Composability and scalability are highly desirable in these simulators to provide design candidates. This section scans over different energy converter scaling approaches adopted by researchers and simulators in the past. This section also includes an in-depth Willans line scaling model for engines and electric machines. The prior knowledge to understand Willans line model is also mentioned.

2.4.1 Scaling Methods

The Powertrain System Analysis Toolkit (PSAT) is a “forward-looking” model, PSAT allows users to simulate more than 200 pre-defined configurations, including conventional, pure electric, fuel cell, and hybrids (parallel, series, power split, series-parallel). The simulator was developed by Argonne National Laboratory (ANL) and sponsored by the U.S. Department of Energy (DOE) [18]. ADvanced VehIcle SimulatOR (ADVISOR) is another simulator but unlike PSAT, ADVISOR is a “backward-looking” simulator, which can be used for the analysis of performance, fuel economy, and emissions of conventional, electric, hybrid electric, and fuel cell vehicles. ADVISOR was developed by U.S. National Renewable Laboratory (NREL) [18]. ADVISOR and PSAT are based in MATLAB/Simulink environment. Both the simulators, utilize engine’s fuel consumption and efficiency data to evaluate the overall performance of the vehicle. The data within these simulators is in the form of look-up tables within MATLAB. Based on the maximum power and efficiency of the desired engine, both the simulators (PSAT and ADVISOR) employ linear scaling strategy, which allows the user to conduct parametric studies for the options that are not on the list of available engines within the simulator. In other words, when a chosen engine has either different maximum power rating or different peak efficiency from the default values, their efficiency maps will be proportionally scaled with the efficiency ratio. Speed and torque indices of the efficiencies are also scaled based on the required maximum power of the engine.

Assanis *et al.* [19] apply a different scaling strategy to a high-fidelity turbocharged compression-ignition engine simulator. The scaling done by [19] provides better prediction

of the fuel consumption and efficiency data for the scaled engines because the methodology considers non-linearity factors. The high-fidelity of the method makes it more complicated as it requires more knowledge of many engine parameters.

J. Pries and H. Hoffmann [20] provide a way that allows magnetic and thermal scaling of electric machines. The method adopted by [20] involves developing partial differential equations describing electromagnetic and thermal dynamics of the machine, which incorporate non-linear magnetic behavior such as saturation and hysteresis. The high-fidelity of the method makes it more complicated than the scope of this project.

In the past, Willans line model has been used to describe an approximate linear relationship between brake mean effective pressure and fuel consumption of an ICE. [12] Rizzoni, Guzzella and Baumann [11] extended the already existing Willans line model to describe generalized energy converters (engines and electric motors). Based on known steady state efficiency data of the reference machine, the efficiency of a new machine in the same category can be estimated using this scaling approach.

The Willans line model consists of an affine relationship which relates the available energy, that is, the energy that is theoretically available for conversion, to the useful energy that is actually present at the output of the energy converter. The relationship is described by two coefficients: the slope, or intrinsic energy conversion efficiency e; and the vertical axis intercept W_{loss}. In an ICE, e corresponds to the energy conversion efficiency that is characteristic of a specific cycle (Otto, Diesel, Miller, *etc.*) and W_{loss} represents the frictional and auxiliary losses [11]. The relationship is described in Equation (2.2) and a representation of that relation is shown in Figure 15.

$$W_{out} = eW_{in} - W_{loss} \tag{2.2}$$

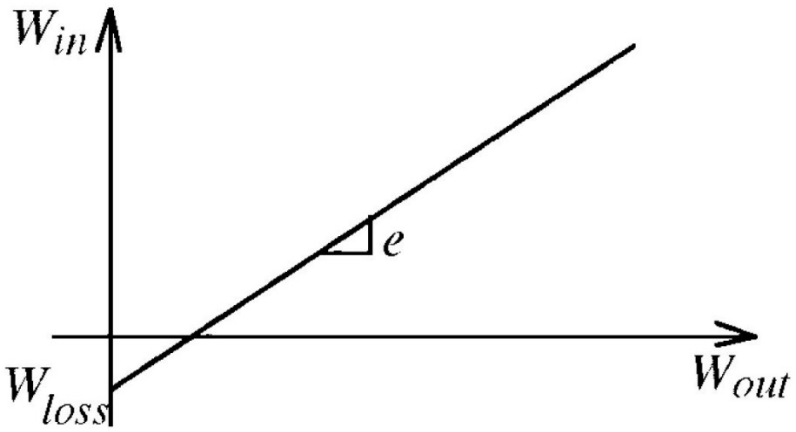

Figure 15: Input-Output Relationship of an Energy Converter [11]

The actual energy conversion efficiency of an energy converter can be defined as the ratio of output work done to the input work done by the converter as described in Equation (2.3).

$$\eta = \frac{W_{out}}{W_{in}} \tag{2.3}$$

Relating equations (2.2) & (2.3) indicate that the actual conversion efficiency is a function of the operating conditions of the converter and that it is maximum in that operating region where the ratio of energy losses to input energy is smallest.

$$\eta = \frac{eW_{in} - W_{loss}}{W_{in}} = e - \frac{W_{loss}}{W_{in}} \tag{2.4}$$

Further application of the Willans line concept to the engine and electric machines scaling, and also the method adopted to predict e and W_{loss} for the two is energy converters is explained in the section.

2.4.1.1 Engine Fuel Consumption and Efficiency Maps

The fuel consumption and efficiency maps of an engine are contour plots based on experimental engine fuel consumption and power output data, which are usually indexed by engine operating torque and speed. The data used in these maps is obtained at steady state and thus the maps do not represent engine dynamic behaviors.

Figure 16 and Figure 17 show the fuel consumption and efficiency maps of a 1.9 L diesel turbocharged engine respectively. It is evident from the fuel consumption map that engines consume more fuel under higher load, *i.e.*, higher speed or higher torque or both. From looking at Figure 17 it is clear that the engine operates at its peak efficiency at a relatively lower speed and higher torque. It is more convenient to use the fuel consumption map when calculating vehicle fuel economy of the vehicle.

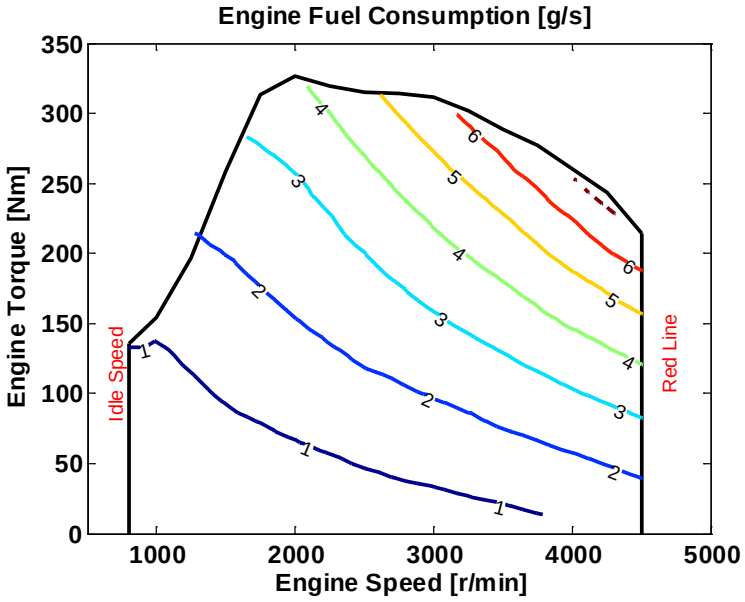

Figure 16: Fuel Consumption Map of a 1.9 L Turbocharged Diesel Engine

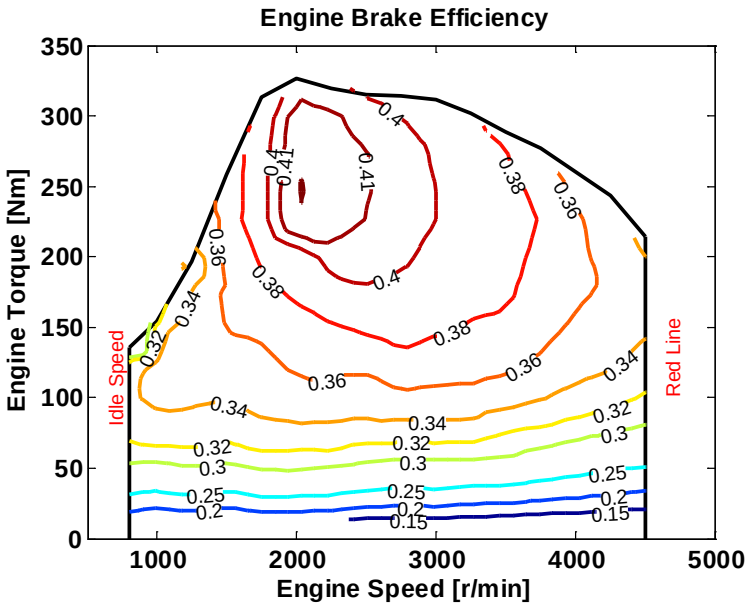

Figure 17: Efficiency Map of a 1.9 L Turbocharged Diesel Engine

The engine fuel consumption map is interchangeable with the engine efficiency map, in the sense of describing engine losses. According to Equation (2.5) through Equation (2.7), the two maps can be easily converted to each other as long as the fuel's lower heating value Q_{LHV} is known.

$$P_{in(ice)} = \dot{m}_f * Q_{LHV} \tag{2.5}$$

$$P_{out(ice)} = T_{ice} * \omega_{ice} \tag{2.6}$$

$$\eta_{ice} = \frac{P_{out(ice)}}{P_{in(ice)}} \tag{2.7}$$

Where,

$P_{in(ice)}$ Engine input power (W),

$\dot{m}_f$ Engine mass flow rate of fuel (kg/s),

Q_{LHV} Lower heating value of the fuel (J/kg),

$P_{out(ice)}$ Engine output power (W),

T_{ice} Engine torque (N-m),

ω_{ice} Engine speed (rad/s),

η_{ice} Engine efficiency.

2.4.1.2 Willans Line Model for Engines

The input-output powers and the intrinsic efficiency of an engine, as viewed for the Willans line model is described in Equation (2.8).

$$P_{out(ice)} = e_{ice} * P_{in(ice)} - P_{loss(ice)} \tag{2.8}$$

In order to eliminate sizing effects, the engine speed and the torque are substituted by the normalized variables including the mean piston speed and the mean effective pressures. According to [12], torque is a valuable measure of a particular engine's ability to do work which, depends on engine size. A more useful relative engine performance measure is obtained by dividing the work per cycle by the cylinder volume displaced per cycle as expressed in Equation (2.11). Also, [12] states that mean piston speed is often a more appropriate parameter than crank rotational speed for correlating engine behavior as a function of speed. The instantaneous piston velocity Cm is obtained from the Equation (2.9). Figure 18 represents the physical parameters (stroke length and displacement volume) of the engine that have been used in the Equation (2.9) through Equation (2.11).

$$C_{m(ice)} = \frac{S * \omega_{ice}}{\pi} \tag{2.9}$$

$$P_{ma(ice)} = \frac{4\pi Q_{LHV}\,\dot{m}_f}{V_d \omega_{ice}} \tag{2.10}$$

$$P_{me(ice)} = \frac{4\pi T_{ice}}{V_d} \tag{2.11}$$

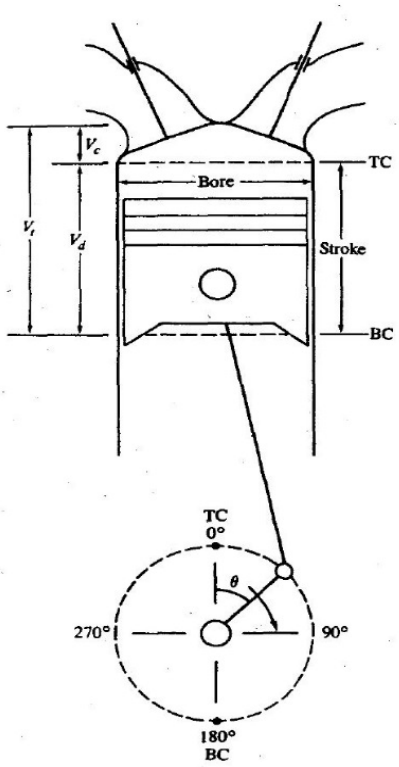

Figure 18: Geometry of Cylinder, Piston, Connecting Rod and Crankshaft in an Engine [12]

Hence, the energy conversion efficiency with the normalized parameters becomes

$$\eta_{ice} = \frac{P_{me(ice)}}{P_{ma(ice)}} \tag{2.12}$$

Now, the input-output relationship according to Willans line model for engines can be written in the format represented in Equation (2.13).

$$P_{me(ice)} = e_{ice} * P_{ma(ice)} - P_{ml(ice)} \tag{2.13}$$

Once, $P_{ma(ice)}$ and $P_{me(ice)}$ are calculated at each operating speed, the intrinsic efficiency e_{ice} and the mean friction pressure $P_{ml(ice)}$ are approximated to be functions of $C_{m(ice)}$ and $P_{ma(ice)}$ as represented in Equation (2.14) and Equation (2.15) respectively.

$$e_{ice} = \left(e_{00(ice)} + e_{01(ice)} C_{m(ice)} + e_{02(ice)} C^2_{m(ice)}\right) - \left(e_{10(ice)} + e_{11(ice)} C_{m(ice)}\right) P_{ma(ice)} \tag{2.14}$$

$$P_{ml(ice)} = P_{ml0(ice)} + P_{ml2(ice)} C^2_{m(ice)} \tag{2.15}$$

$e_{10(ice)}$ and $e_{11(ice)}$ in Equation (2.14) are often close to zero, reducing e_{ice} to a function of $C_{m(ice)}$ alone. The wide-open throttle mean effective pressure curve of engines is identified as shown in Equation (2.16).

$$P_{\max(ice)} = \sum_{i=0}^{3} P_{maxi(ice)} C^i_{m(ice)} \tag{2.16}$$

In Equations (2.8) through (2.16),

$C_{m(ice)}$	Engine mean piston speed (m/s),
$P_{loss(ice)}$	Engine power losses (W),
S	Engine stroke length (m),
$P_{ma(ice)}$	Engine theoretically available mean effective pressure (Pa),
V_d	Engine displacement (m^3),

$P_{me(ice)}$ Engine actual mean effective pressure (Pa),

$P_{ml(ice)}$ Engine mean friction pressure (Pa),

e_{ice} Engine intrinsic energy conversion efficiency - transferring losses (%),

$e_{ij(ice)}$ Scaling coefficients of engine intrinsic energy conversion efficiency e_{ice},

$P_{mli(ice)}$ Scaling coefficients of engine mean friction pressure,

$P_{\max(ice)}$ Engine wide-open throttle mean effective pressure (Pa),

$P_{\text{maxi}(ice)}$ Scaling coefficients of wide-open throttle mean effective pressure.

Two important things need to be noted when applying the Willans line model. First, the scaled machine and the scaling machine should be from the same class of engines, e.g. SI or CI engines, turbo/supercharged engines. Further, when generating the scaling coefficients, the user should curve fit over a wide range of the scaling variable of $C_{m(ice)}$ so that during the subsequent use of the model, the efficiency of the scaled engine is not obtained by doing extrapolation [11].

2.4.1.3 Electric Machine Efficiency Map

The efficiency map which is not restricted to the machine type finds extensive applications in solving automotive design and control problems. Similar to the engine efficiency map, the EM efficiency map also represents static empirical efficiency data as contours on a torque-speed plot. Figure 19 shows the efficiency map of a brushless PM motor with a rotor volume of 1.4 L.

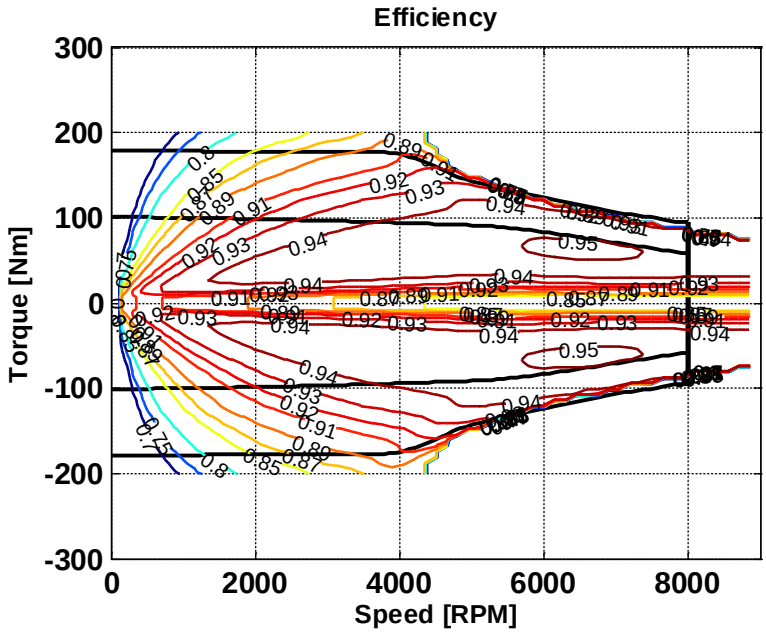

Figure 19: PM Brushless Motor with a 1.4 L Rotor Efficiency Map

The flat segment in the maximum torque curve as mentioned in Section 2.3.2 is called constant torque region and the hyperbolic decaying segment reflects the flux weakening region. Unlike Figure 11 it can be seen that the torque in Figure 19 is positive as well as negative. The positive torque region shows the propulsion aspect of the EM, *i.e.* the part which converts electrical energy from the battery to mechanical energy which moves the vehicle. The negative torque region shows the regenerative aspect of the EM, *i.e.* the part where the motor converts mechanical energy during braking from the wheels to electrical energy to charge the battery pack in a HEV or an EV. The EM behavior in the generating mode (negative EM torque region) is usually different from those in the motoring mode (positive EM torque region), but engineers may consider they are the same, *i.e.*, symmetric about the zero torque line for

simplicity. In general, the highest efficiency of an EM is located at the higher power region.

2.4.1.4 Willans Line Model for Electric Machines

As mentioned earlier, the Willans line model is also applicable in describing electric machines. The input-output powers and the efficiency of an EM in the motoring mode are described in Equation (2.17) through Equation (2.19).

$$P_{in(em)} = U * I \tag{2.17}$$

$$P_{out(em)} = T_{em} * \omega_{em} \tag{2.18}$$

$$\eta_{em} = \frac{P_{out(em)}}{P_{in(em)}} \tag{2.19}$$

Using the Willans line concept, the EM input-output relationship can be represented as is done in Equation (2.20).

$$P_{out(em)} = e_{em} * P_{in(em)} - P_{loss(em)} \tag{2.20}$$

Applying the normalized variables of the mean rotor speed and the air gap shear stresses, we obtain:

$$C_{m(em)} = r_r \omega_{em} \tag{2.21}$$

$$P_{ma(em)} = \frac{U * I}{2V_r \omega_{em}} \tag{2.22}$$

$$P_{me(em)} = \frac{T_{em}}{2 * V_r} \tag{2.23}$$

$$\eta_{em} = \frac{P_{me(em)}}{P_{ma(em)}} \tag{2.24}$$

$$P_{me(em)} = e_{em} * P_{ma(em)} - P_{ml(em)} \tag{2.25}$$

The physical parameters (rotor radius and rotor length) used in Equation (2.21) through Equation (2.23) are described in Figure 20.

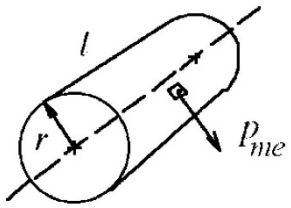

Figure 20: Rotor Physical Parameters

Noting the success of the polynomial models for the engine, polynomials in $C_{m(em)}$ were initially selected to model e_{em} and $P_{ml(em)}$ of the EM according to [11]. Again according to [11] the simulation results showed that fourth order polynomials capture the behavior of e_{em} and $P_{ml(em)}$ with sufficient accuracy and without excessive coefficients, the expressions for which are illustrated in Equation (2.26) and Equation (2.27) respectively.

$$e_{em} = \sum_{i=0}^{4} e_{0i(em)} C_{m(em)}^{i} \tag{2.26}$$

$$P_{ml(em)} = \sum_{i=0}^{4} P_{mli(em)} C_{m(em)}^{i} \tag{2.27}$$

In Equation (2.17) through Equation (2.27),

$P_{in(em)}$ EM input power (W),

$P_{loss(em)}$ EM power losses (W),

U EM voltage supply (V),

I EM current supply (A),

$P_{out(em)}$ EM output power (W),

$C_{m(em)}$ EM mean rotor speed (m/s),

r EM rotor radius (m),

$P_{ma(em)}$ EM theoretical air gap shear stress (Pa),

V_r EM rotor volume (m^3),

$P_{me(em)}$ EM actual air gap shear stress (Pa),

$P_{ml(em)}$ EM mean friction pressure (Pa),

e_{em} EM intrinsic energy conversion efficiency - transferring losses (%),

$e_{ij(em)}$ Scaling coefficients of EM intrinsic energy conversion efficiency e_{ice},

$P_{mli(em)}$ Scaling coefficients of EM mean friction pressure,

The Willans line model for the electric machines also allows building the scalable models within the same category, such as induction EM, permanent magnet synchronous EM and switched reluctance EM. One may refer to engine's Willans line model for detailed description of model application and restrictions.

2.5 EcoSIM

The Ohio State EcoCAR team has developed an energy-based model called EcoSIM to develop control strategies for the vehicle over the past 8 years. This model allows the team to see how different strategies affect fuel economy and performance. This

chapter contains a very basic explanation of this model. A more detailed description can be found in [4].

2.5.1 Overview

EcoSIM consists of 4 major subsystems: the driver, supervisory control, powertrain, and the vehicle dynamics subsystems. EcoSIM is a "forward-looking" model where, the driver subsystem acts as the human driver would in real life, this subsystem changes the brake and accelerator pedal position based on the desired speed based on a predetermined drive cycle. Based on the pedal positions provided by the driver, the supervisory control subsystem determines an appropriate torque and speed request for the powertrain components. These requests are then sent to the powertrain subsystem which contains the component level controllers and plant models. This subsystem then outputs a total tractive force that the tires exert on the road which is fed into a vehicle dynamics subsystem which determines vehicle speed. This speed is then fed back into the driver subsystem. A top-level diagram of the EcoSIM is shown in Figure 21.

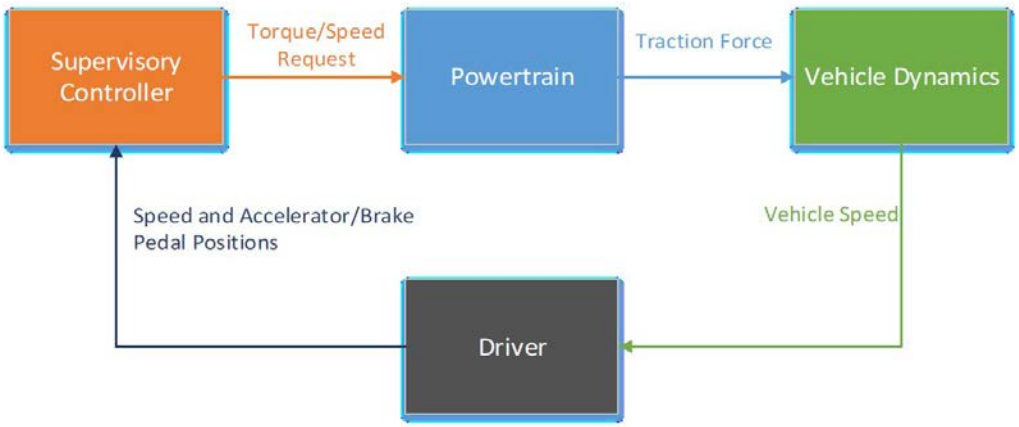

Figure 21: EcoSIM Top Level Structure

Within the powertrain subsystem, engines' and electric machines' controllers and plant models are stored. The engine plant model includes simplified dynamics of the engine torque and speed response and output the actual torque and speed. With this torque and speed it is possible to find the engine efficiency and engine fuel consumption rate based on the maps which are stored within EcoSIM in the form of look-up tables. Similarly, once the EM torque and speed commands are determined, they get passed to the EM plant model which contains simplified dynamics. The plant model then outputs a torque and speed. From this, the efficiency of the EM can be determined using stored efficiency maps. It is these fuel consumption and efficiency maps of the engines and electric machines that the EcoCAR 3 team would replace with different size engine and EM data to test different components.

CHAPTER 3: SCALING METHODS

3.1 Introduction

The methods utilized by the developed tools to scale engine and electric machine's data, which will be used by the EcoCAR 3 team to test different size components within EcoSIM, and the assumptions made during scaling of these energy converters data are described in this chapter.

3.2 Engine Scaling

The engine-scaling tool was developed within MATLAB. The tool allows the user to generate fuel consumption and power output data of an engine of desired size given the fuel consumption data of an already existing engine (of different size) belonging to the same category. The same category restriction means if the user wants to generate data for a certain type of engine (naturally aspirated, super/turbo-charged, gasoline direct injection, SI, CI, *etc.*) the tool will require the fuel-consumption data for that same type of already existing engine. This requirement of the tool has been explained in Section 2.3.1 of this thesis. Any change in the engine technology affects the engine performance significantly. The scaling method adopted by the engine-scaling tool for this project is very similar to the Willans line model, which has been explained in section 2.4.1.2. The difference between the approach adopted by this project and the Willans line model is that this tool assumes the efficiencies of engines with similar technologies to be the same. Due to this assumption the tool developed can scale engines that are within thirty percent size range of the baseline engine. The accuracy of the predicted data decreases as the size difference

between the baseline engine and the required engine increases more than thirty percent. Since, the difference between displacements of the engines under consideration by the EcoCAR 3 team is within thirty percent, this restriction of the scaling tool is not of concern to the EcoCAR 3 team. The step-by-step scaling of a 1.6 L Naturally Aspirated (NA) SI engine to a 1.8 L NA-SI engine and the comparison between the 2 engines is illustrated further in this section.

As mentioned earlier, the engine-scaling tool requires fuel consumption data of same type already existing engine. Table 1 shows the technological aspect and the physical parameters of the existing engine, the data for which was extracted from PSAT's component library. The Figure 22 shows how the fuel consumption of the 1.6 L engine varies with respect to torque and speed. At each indexed point where the fuel consumption data was available, the power output of the engine was determined using Equation (3.1) and the corresponding map is shown in Figure 23.

$$P_{out(ice)} = T_{ice} \cdot \omega_{ice} \tag{3.1}$$

Table 1: Specifications for the Existing Engine

Engine Technology	**Engine Displacement (V_d) (L)**	**Engine Stroke Length (S) (mm)**
Naturally Aspirated	1.6	90

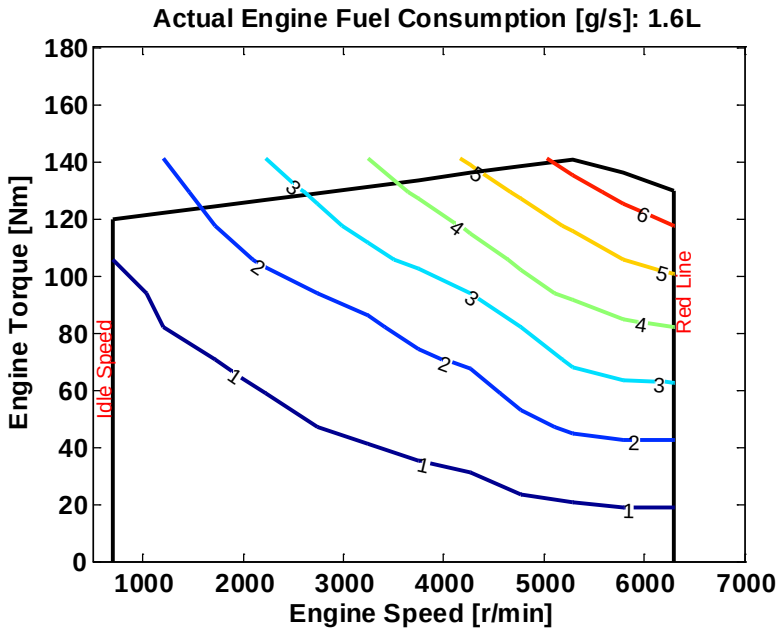

Figure 22: Fuel Consumption Map of a 1.6 L NA-SI Engine

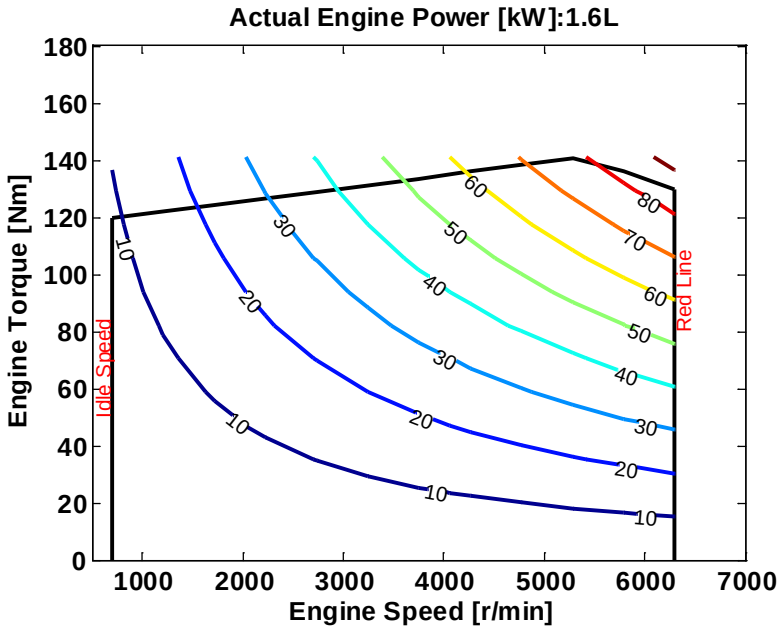

Figure 23: Power Output Map of a 1.6 L NA-SI Engine

Once the power output and fuel consumption of the engine are known, the efficiency of the engine at the same indexed points is determined using Equation (3.2).

Figure 24 represents the efficiency map of the 1.6 L engine.

$$\eta_{ice} = \frac{P_{out(ice)}}{P_{in(ice)}} = \frac{P_{out(ice)}}{\dot{m}_f Q_{LHV}} \tag{3.2}$$

In Equation (3.1) and Equation (3.2):

$P_{in(ice)}$ Engine input power (W),

$\dot{m}_f$ Engine mass flow rate of fuel (kg/s),

Q_{LHV} Lower heating value of the fuel (J/kg),

$P_{out(ice)}$ Engine output power (W),

T_{ice} Engine torque (N-m),

ω_{ice} Engine speed (rad/s),

η_{ice} Engine efficiency

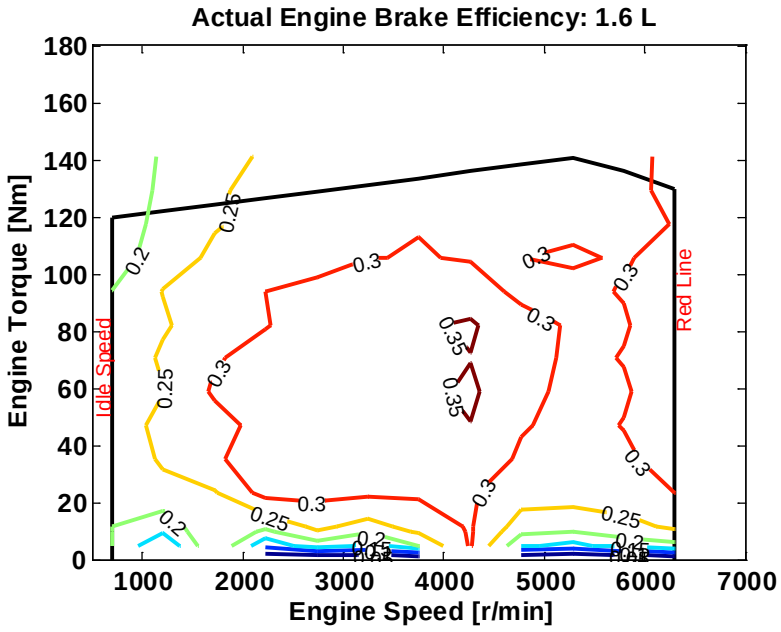

Figure 24: Efficiency Map of a 1.6 L NA-SI Engine

Further the tool converts engine's torque and speed at every efficiency points to normalized parameters *i.e.,* engine's BMEP and mean piston speed respectively. The efficiencies of the engine at these indexed points are kept constant. Figure 25 shows a map of how the engine's efficiency varies with the engine's BMEP and mean piston speed. The mean piston speed and the engine's brake mean effective pressure are calculated using Equation (3.3) and Equation (3.4) respectively.

$$C_m = \frac{S * N}{30} \tag{3.3}$$

$$BMEP = \frac{4\pi T}{100000 * V_d} \tag{3.4}$$

In the equations:

C_m Engine mean piston speed (m/s)

S Engine stroke length (m)

N Engine speed (RPM)

$BMEP$ Engine brake mean effective pressure (bar)

T Engine torque (Nm)

V_d Engine's displacement volume (m^3)

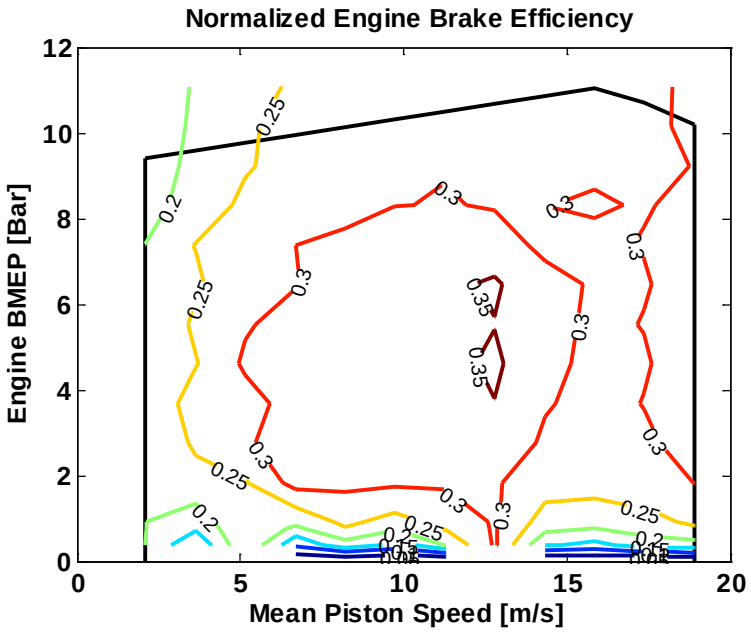

Figure 25: Normalized Efficiency Map of a NA-SI Engine

The data shown in the efficiency map in Figure 25, with the normalized parameters can be utilized to scale any engine with a displacement that is within thirty percent range of the 1.6 L engine. As an example the 1.6 L engine has been scaled to another 1.8 L engine, the specifications for which are described in Table 2.

Table 2: Specifications for the Predicted Engine

Engine Technology	**Engine Displacement (V_{dnew}) (L)**	**Engine Stroke Length (S_{new})(mm)**
Naturally Aspirated	1.8	88.3

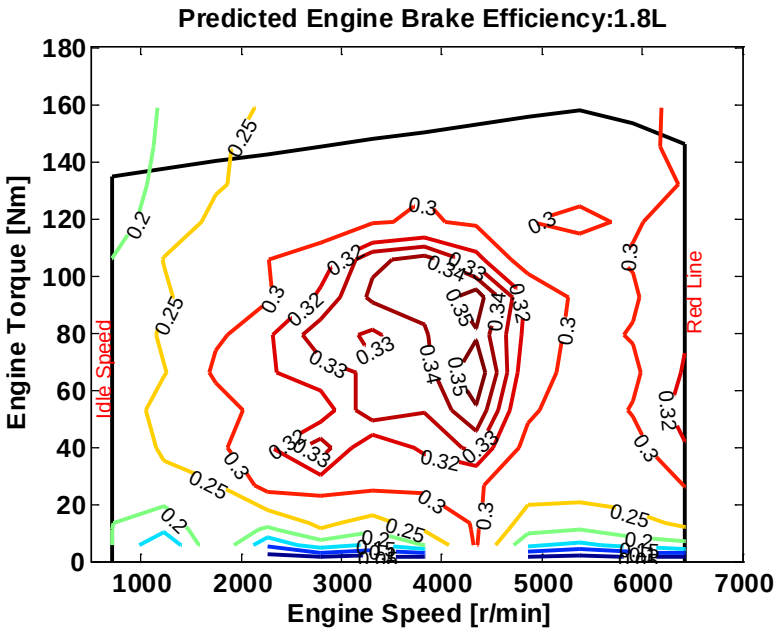

Figure 26: Predicted Efficiency Map of a 1.8L NA-SI Engine

Figure 26 illustrates the brake efficiency of the new NA 1.8 L SI engine. The normalized terms *i.e.* the BMEP and mean piston speed of the 1.6 L engine were used in conjunction with the physical parameters of the 1.8 L engine to determine the new torque and speed indices for the efficiencies. Equation (3.5) and Equation (3.6) describe the conversion of engine BMEP to torque and mean piston speed to engine speed respectively.

$$T_{new} = \frac{BMEP * 10000 * V_{d\,new}}{4 * \pi} \tag{3.5}$$

$$N_{new}\left[RPM\right] = \frac{C_m * 30}{S_{new}} * \frac{1\left[RPM\right]}{.104719\left[\frac{rad}{s}\right]} \tag{3.6}$$

Where, T_{new} and N_{new} are the torque and speed of the newly scaled engine. The converted torques and speed at each of the indexed efficiency points are used to determine the engine power output. Figure 27 illustrates the power output map of the 1.8 L engine.

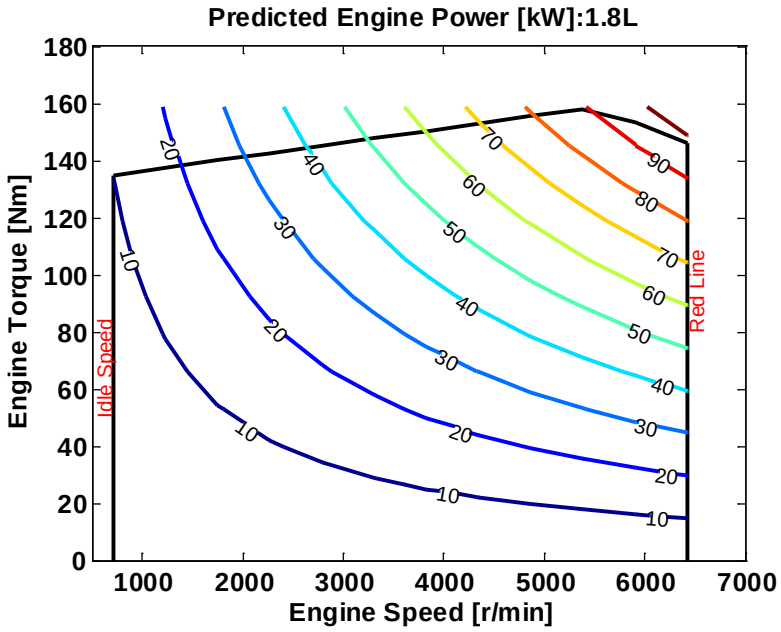

Figure 27: Predicted Power Map of a 1.8L NA-SI Engine

Utilizing the power output and efficiency data points, the fuel consumption of the 1.8L engine was determined using Equation (3.7) and Figure 28 illustrates the predicted fuel consumption map of the 1.8 L engine.

$$\dot{m}_f = \frac{\eta_{ice} * Q_{LHV}}{P_{out(ice)}} \tag{3.7}$$

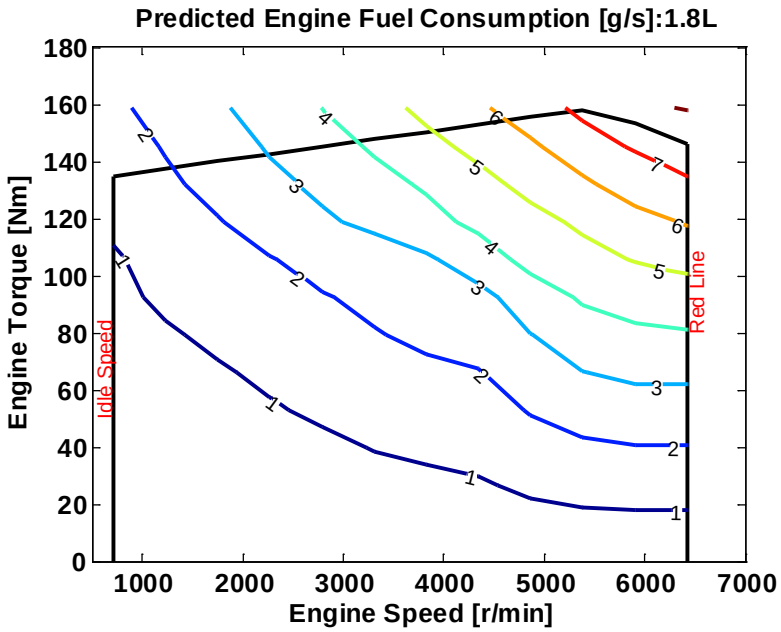

Figure 28: Predicted Fuel Consumption Map of a 1.8L NA-SI Engine

Figure 29 shows a side-by-side comparison of the two engine's fuel consumption, brake efficiency and power output. On the left side of Figure 29 (a, c & e), the fuel consumption, brake efficiency and power output of the original NA 1.6 L SI engine are shown and the same parameters for the 1.8 L engine are on the right side (b, d &f). The trends for all the three parameters look very similar to each other but the values vary. Table 3 lists the two engine's peak torque, peak power output, peak efficiency and peak fuel consumption values and the indexed torque and speed where those points occur on their respective maps.

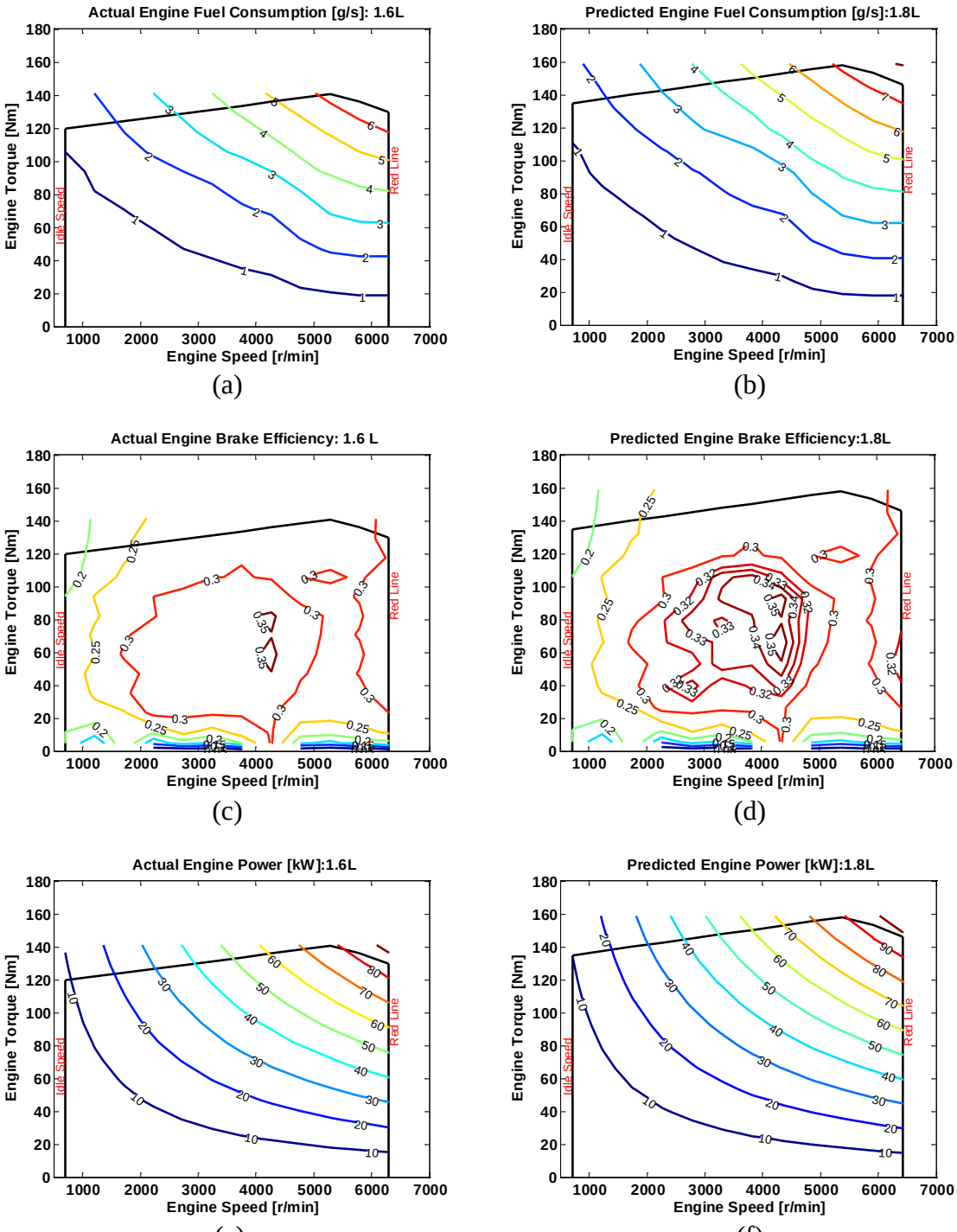

Figure 29: Actual 1.6 L and Predicted 1.8 L engine (a-b) Fuel consumption, (c-d) Efficiency and (e-f) Power Output comparison

Table 3: Original vs. Scaled Engine Parameters Comparison

		NA 1.6 L SI engine		NA 1.8 L SI engine (predicted)		
		Torque (Nm)	Speed (RPM)		Torque (Nm)	Speed (RPM)
Peak Torque (Nm)	140.5	140.5	5282	158	158	5384
Peak Power Output (kW)	85	129.3	6300	97.8	145.4	6421
Peak efficiency	35.89	58.8	4264	35.89	66.1	4345.7
Peak Fuel Consumption (g/s)	6.5	129.3	6300	7.45	145.4	6421

Looking at Table 3 and Figure 29 it can be seen that the peak power and peak fuel consumption of the both the engines occur at the same respective indexed torque and speed. The peak fuel consumption and peak power output value and also the corresponding torque-speed indices where these occur are different for both the engines. The 1.8 L engine has a higher power output and consumes more fuel at its peak points than the 1.6 L engine, proving the tool is scaling the engine in a correct fashion. The maximum torque of the 1.8 L is higher than the original 1.6 L engine and occurs at a faster speed as well. Peak brake efficiencies of the two engines is the same due to the constant efficiency assumption of the tool, while the torque-speed indices for the two engines where the peak efficiency occurs are different. The 1.8 L engine reaches at its peak efficiency at a higher torque and speed as compared to the 1.6 L engine.

3.3 Electric Machine Scaling

Just like the engine-scaling tool the electric machine (EM) scaling tool was developed within MATLAB as well. The tool allows the user to generate efficiency and power output data of an EM of desired size given the efficiency data of an already existing EM (of different size) belonging to the same category. Using the power output and efficiency data, the user could also get the power consumption map of the EM. The same category restriction means if the user wants to generate data for a certain type of EM (DC, IM, brush-less PM motor *etc.*) the tool will require the efficiency data for that same type of already existing engine. This requirement of the tool has been explained in Section 2.3.2 of this thesis-any change in the EM technology affects the EM's torque-speed characteristics significantly. The scaling method adopted by the EM scaling tool for this project is very similar to the Willans line model, which has been explained in Section 2.4.1.4. The difference between the approach adopted by this project and the Willans line model is that this tool assumes the efficiencies of EMs with similar technologies to be the same. Due to this assumption the tool developed can scale EMs that are within a certain percent size range of the baseline EM for which the data is available. The maximum percent difference between the baseline EM and the to-be scaled EM for accurate results is unknown. But it is known that the accuracy of the predicted data decreases as the size difference between the baseline EM and the required EM increases. The step-by-step scaling of a brush-less PM motor with a 1.4 L rotor by volume to a brush-less PM motor with a 2.1 L rotor by volume and the comparison between the 2 EMs is illustrated further in this section.

As mentioned earlier, the EM scaling tool requires the energy conversion efficiency data of same type already existing EM. Table 4 shows the technological aspect and the physical parameters of the existing EM, Parker-Hannifin's GVM210-100-TP**,** the efficiency and performance data for which was provide to the EcoCAR 2 team by Parker-Hannifin. Parker-Hannifin evaluated the parameters within a FEA study, which was further validated by them experimentally.

Table 4: Specifications for the Existing EM

EM Technology	**Rotor Stack Length (l) (mm)**	**Rotor Radius (r) (mm)**
Brush-less PM motor	100	66.75

Further the physical parameters provided were used to determine the volume of the EM's rotor using the Equation (3.8) and found to be 1,369,980 mm^3.

$$V_r = \pi r^2 l \tag{3.8}$$

Figure 30 shows how the energy conversion efficiency of the EM with a 1.4 L rotor varies with respect to torque and speed. As explained earlier in Section 2.4.1.3 the positive torque region of Figure 30 illustrates when the motor operates during vehicle propulsion (electrical to mechanical) and the negative torque region represents when the motor is taking advantage of the regenerative braking (mechanical to electrical). At each indexed point where the efficiency data was available, the power of the EM was determined using Equation (3.9) and the corresponding power map is shown in Figure 31.

$$P_{(em)} = T_{em} * \omega_{em} \tag{3.9}$$

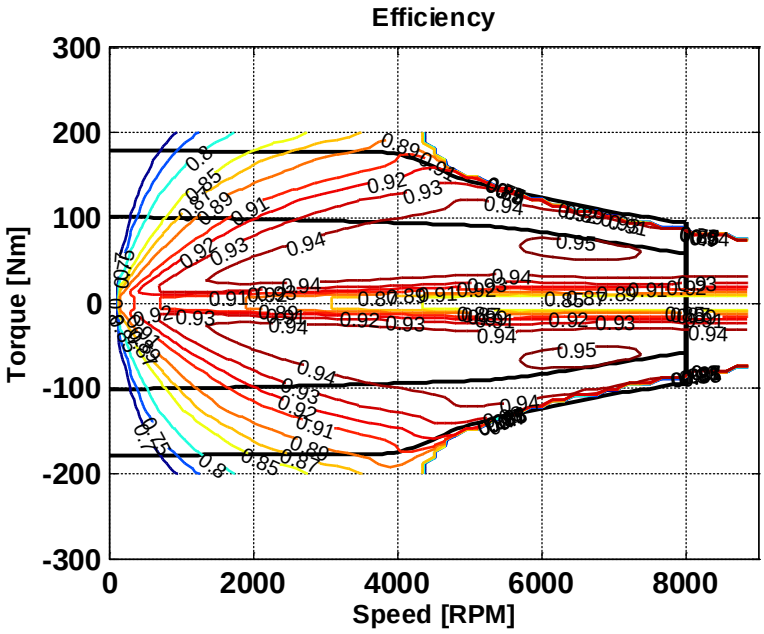

Figure 30: Energy Conversion Efficiency for Existing Brushless PM Motor

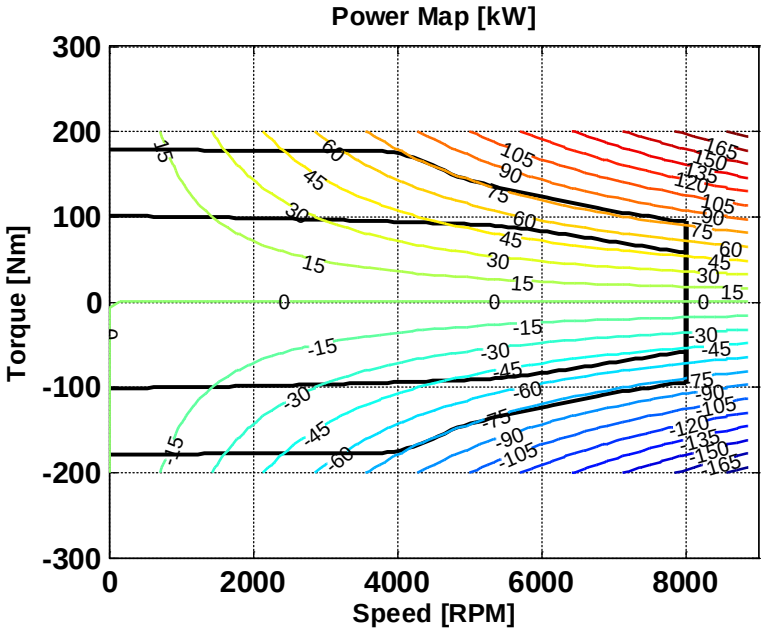

Figure 31: Power Map for Existing Brushless PM Motor

The tool also converts the EM's torque and speed at every efficiency point to normalized parameters *i.e.*, EM's air gap shear stress and mean rotor speed respectively. The efficiencies of the EM at these indexed points are kept the same. Figure 32 shows a map of how the EM's efficiency varies with the EM's air gap shear stress and mean rotor speed. The EM's air gap shear stress and mean rotor speed are calculated using Equation (3.10) and Equation (3.11) respectively.

$$P_{me(em)} = \frac{T}{2 * V_r} \tag{3.10}$$

$$C_{m(em)}\left[m/s\right] = (r * N\left[RPM\right] * \frac{0.104719\left[\frac{rad}{s}\right]}{1\left[RPM\right]} \tag{3.11}$$

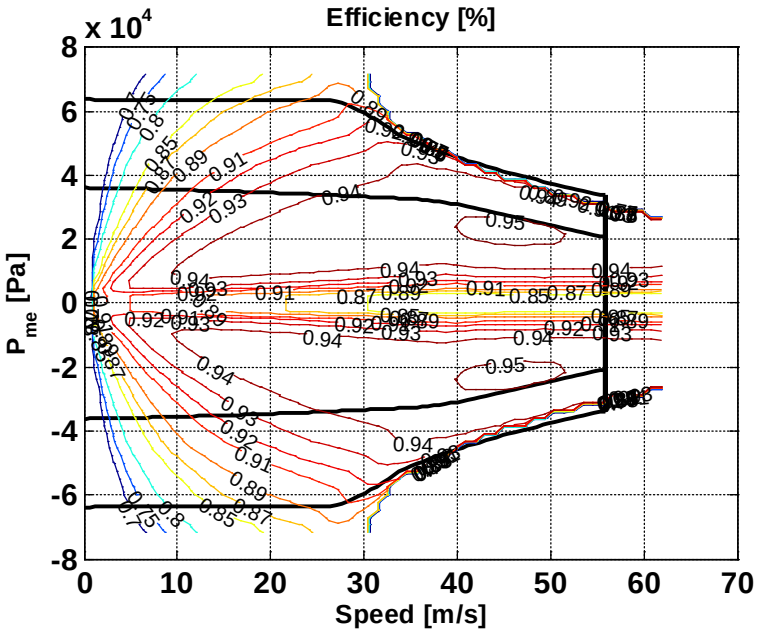

Figure 32: Normalized Efficiency Map of a Brushless PM Motor

The data shown in the efficiency map shown in Figure 32 with the normalized parameters can be utilized to scale any brushless PM motor data. As an example, the EM with the 1.4 L rotor has been scaled to another EM with a 2.1 L rotor, the specifications for which are described in Table 5.

Table 5: Specifications of the Predicted EM

EM Technology	Rotor Stack Length (l) (mm)	Rotor Radius (r) (mm)
Brush-less PM motor	150	66.75

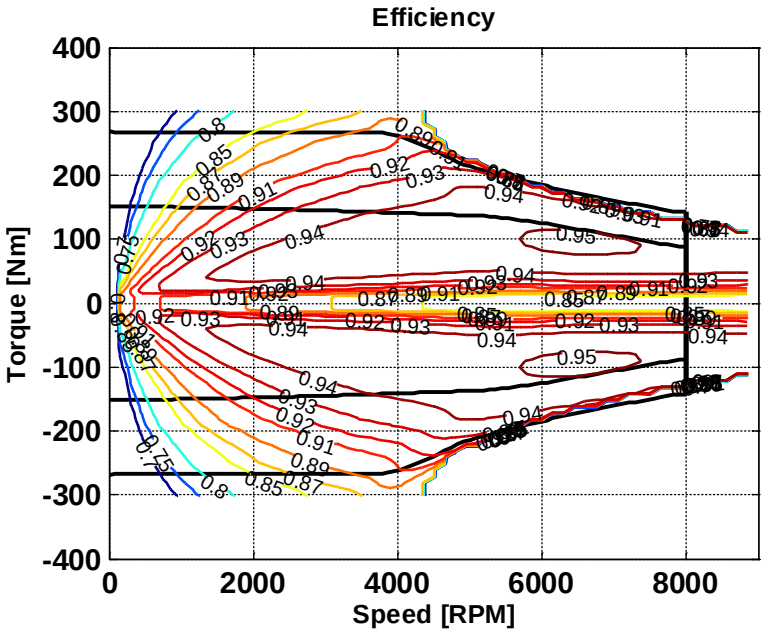

Figure 33: Predicted energy conversion efficiency map for brushless PM motor

Figure 33 illustrates the efficiency of the new brushless PM motor. The normalized terms *i.e.*, the air gap shear stress and the mean rotor speed obtained from 1.4 L rotor EM were used in conjunction with the physical parameters of the 2.1 L rotor EM to determine

the new torque and speed indices for the energy conversion efficiencies for the 2.1 L rotor motor. Equation (3.12) and Equation (3.13) describe the conversion of EM's air gap shear stress to torque and EM's mean piston speed to EM speed respectively.

$$T_{new} = P_{me(em)} * 2 * V_{r\,new} \tag{3.12}$$

$$N_{new}\left[RPM\right] = \frac{C_{m(em)}}{r_{new}} * \frac{1\left[RPM\right]}{.104719\left[\frac{rad}{s}\right]} \tag{3.13}$$

Where, T_{new} and N_{new} are the torque and speed of the newly scaled EM. The converted torques and speeds at each of the indexed efficiency points are multiplied together to determine the EM power. Figure 34 illustrates the power map of the brushless PM motor with a 2.1 L rotor.

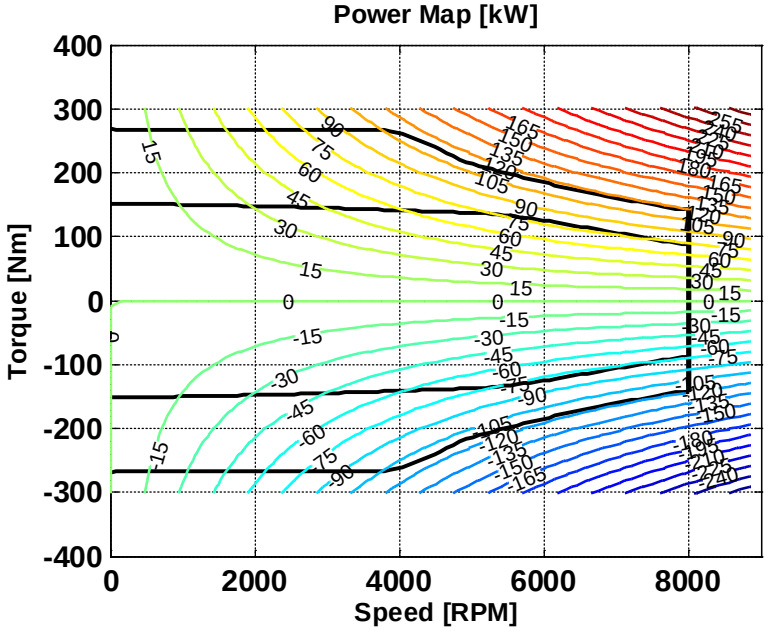

Figure 34: Predicted Power Map for Brushless PM Motor

Figure 35 shows a side-by-side comparison of the two EM's energy conversion efficiency and power map. On the left side of Figure 35 (a & c), the energy conversion efficiency and power map of the original brushless PM motor with a 1.4 L rotor are shown and the same parameters for the 2.1 L rotor motor are on the right side (b & d). The trends for the two parameters look very similar to each other but the values vary. Table 6 lists the two EM's peak torque, peak power output, peak efficiency and stall continuous torque values and the indexed torque and speed where those points occur on their respective maps. Looking at Table 6 and Figure 35 it can be seen that the motor with 2.1 L rotor has a higher power output, higher peak and stall continuous torque but the same peak speed when compared to the EM with 1.4L L rotor, proving the tool is scaling the EM's in a correct fashion. The same speed is due to the no change in the radius of the predicted motor's rotor. Peak energy conversion efficiencies of the two EMs is the same due to the constant efficiency assumption of the tool, while the torques of the torque-speed indices for the two EMs where the peak efficiency occurs are different and the speeds are the same. The EM with 2.1 L rotor engine reaches at its peak efficiency at a higher torque as compared to the EM with a 1.4 L rotor but both the indices have common speed of 6600 RPM, this could be also due to the reason that the no change in the radius of the predicted motor's rotor.

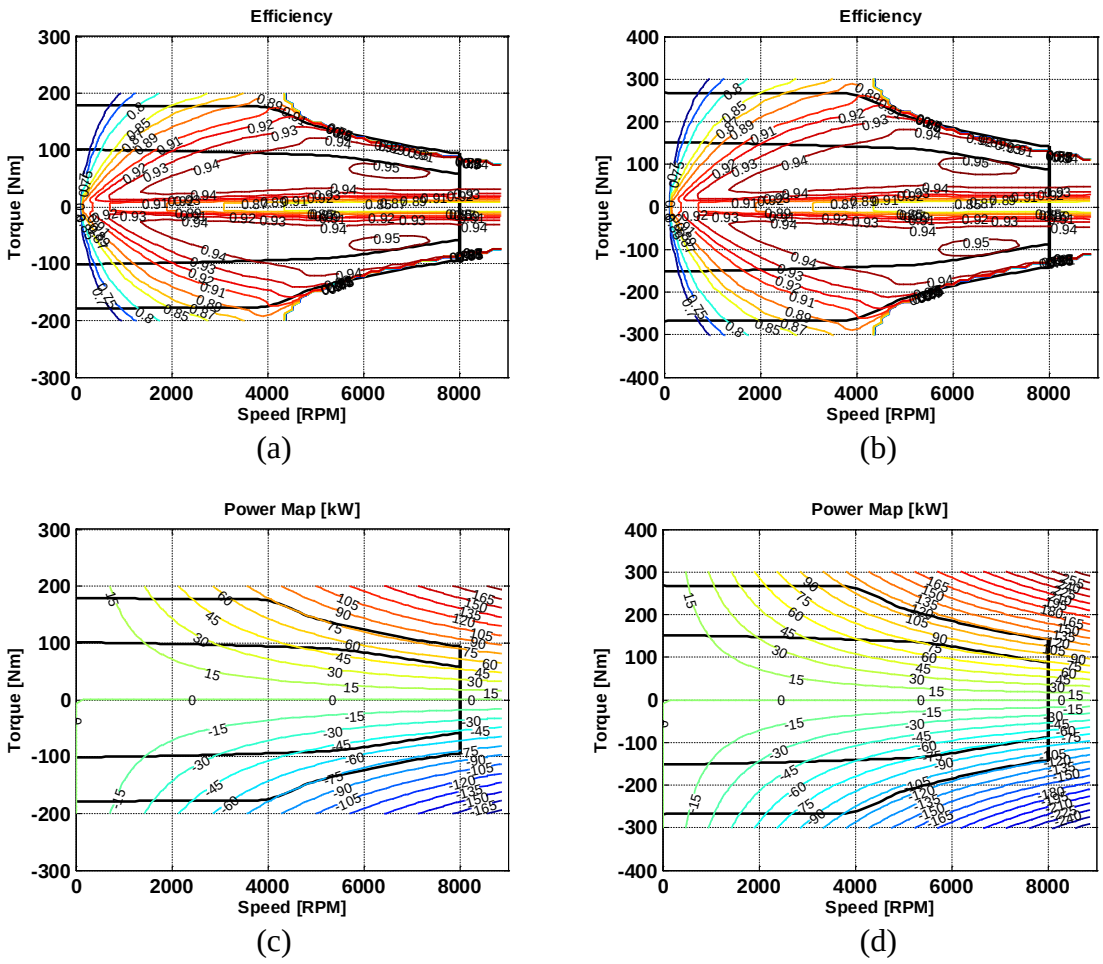

Figure 35: Actual 1.4 L and Predicted 2.1 L Rotor Volume EM's (a-b) Energy Conversion Efficiency, (c-d) Power Map Comparison

Table 6: Original vs. Scaled EMs' Parameters Comparison

	Brushless PM motor (1.4 L rotor)			Brushless PM motor (2.1 L rotor)		
		Torque (Nm)	Speed (RPM)		Torque (Nm)	Speed (RPM)
Peak Torque (Nm)	180	180	0-4000	270	270	0-4000
Peak Power Output (kW)	75	180-95	4000-8000	115	270-143	4000-8000
Peak efficiency	95	60	6600	95	90.5	4345.7
Peak Stall Continuous Torque (Nm)	100	100	-	152	145.4	-

CHAPTER 4: SCALING VALIDATION

4.1 Introduction

The methods utilized by the developed tools to scale engine and electric machine data and the results obtained from these tools, which are described in Chapter 2:, needed to be validated. This had to be done so as to be sure that the EcoCAR 3 team can use the tools developed in this project to scale different components and use the scaled data within EcoSIM to get accurate results. The statistical analysis done to compare how close the scaled data is to the real data for both the kinds of energy converters is explained in this chapter.

4.2 Engine Scaling

To validate the engine scaling method adopted by this project, two comparisons are done. To make comparisons, multiple sets of different engine data are required. The fuel consumption data for existing engines available through the PSAT were: 1.6 L NA-SI engine and two 1.8 L NA-SI engines ((1) & (2)). This project scaled another 1.8 L NA-SI engine, from the 1.6 L engine, using the tool developed in this project as shown in 3.2. The scaled 1.8 L engine had the same physical parameters (displacement volume and stroke length) as the already existing 1.8 L NA-SI engine (1). The fuel consumption and efficiency data of the two existing 1.8 L NA-SI engines ((1) & (2)) are compared against each other. Secondly, the predicted fuel consumption and efficiency data of the scaled 1.8 L engine are compared against the fuel consumption and efficiency data of the actual 1.8 L engine

(1), both of which have the same physical parameters. Figure 36 shows all the data available and the dotted lines around the boxes show the comparisons done for this project.

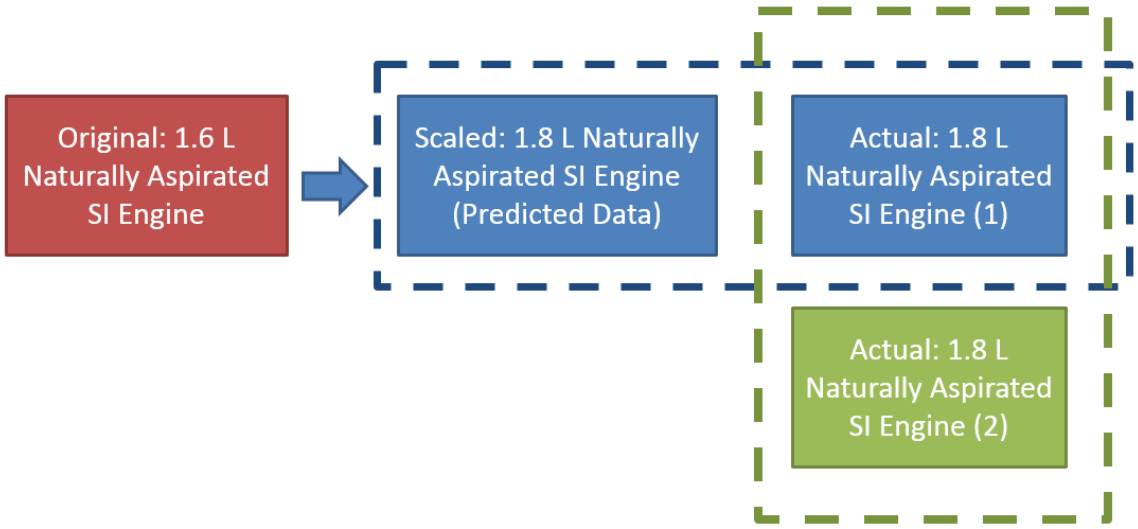

Figure 36: Engine Comparisons

4.2.1 Actual vs. Actual Engines' Comparison

As mentioned earlier, the two 1.8 L NA-SI engines ((1) & (2)) are compared first. Figure 37 shows a side-by-side comparison of the fuel consumption and brake efficiency of the two actual 1.8 L NA-SI engines ((1) & (2)). On the left side of Figure 37 (a & c), the fuel consumption and brake efficiency of 1.8 L engine (1) are shown and the same parameters for the 1.8 L engine (2) are on the right side (b & d). Table 7 lists the two engines' peak torque, peak power output, peak efficiency, and peak fuel consumption values and the indexed torque and speed where those points occur on their respective maps.

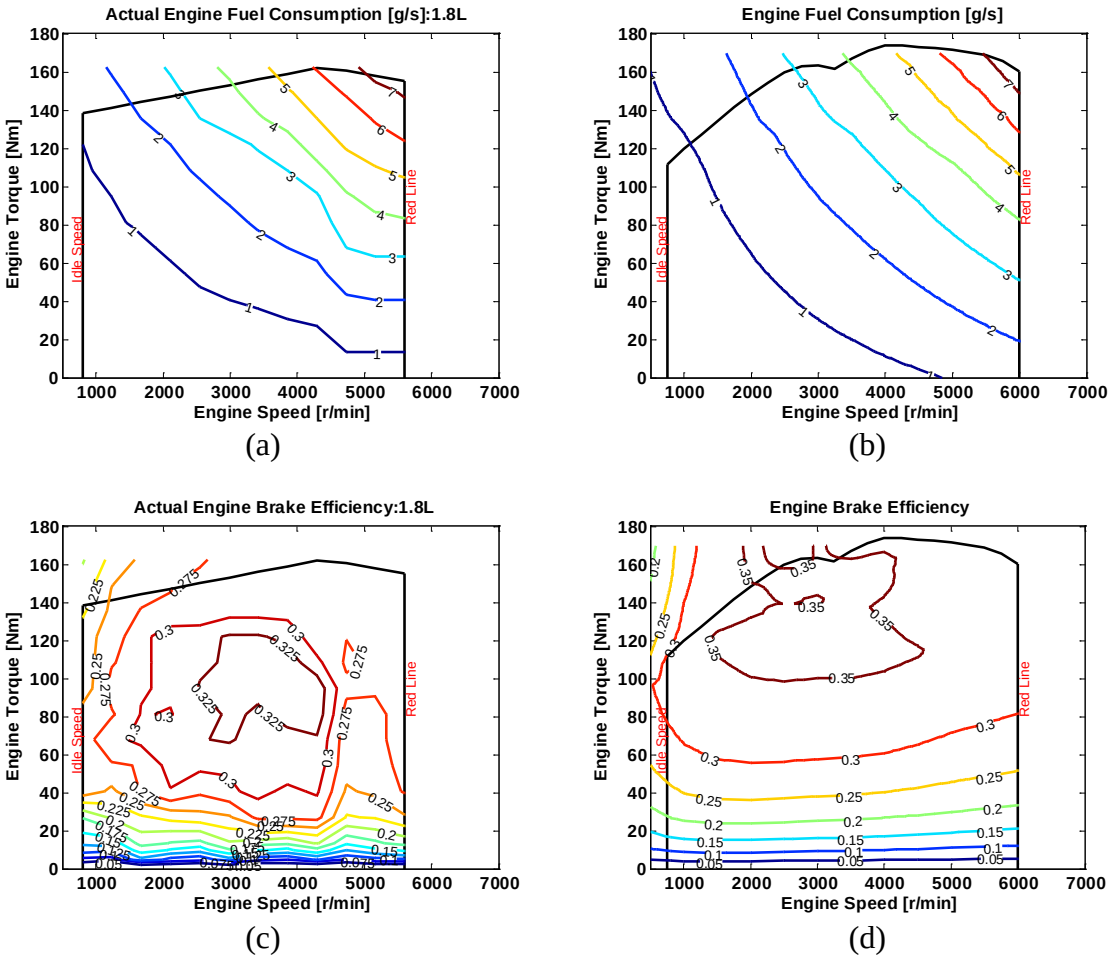

Figure 37: Actual Engines (1&2) (a&b) Fuel Consumption and (c&d) Efficiency Comparison

Table 7: Actual 1.8 L NA-SI Engines' Parameters Comparison

	NA 1.8 L SI engine (1)			NA 1.8 L SI engine (2)		
		Torque (Nm)	Speed (RPM)		Torque (Nm)	Speed (RPM)
Peak Torque (Nm)	162	162	4290	174	174	4000
Peak Power Output (kW)	90	155	5600	99	158	6000
Peak efficiency	33.94	108.5	3855	35.4	144.38	3500
Peak Fuel Consumption (g/s)	7.5	155	5600	7.4	158	6000

Looking at Table 7 and Figure 37 it can be seen that the peak power and peak fuel consumption of the both the engines occur at the same indexed torque and speed of the respective engines. The peak power output value and also the corresponding torque-speed indices where it occur are different for both the engines but the peak fuel consumption is about the same. The 1.8 L engine (2) has a higher power output as well as a higher peak torque but it consumes less fuel at its peak points than the 1.8 L engine (1). Also, engine (2) has a higher peak efficiency value than engine (1), which occurs at a much higher torque than engine (1). This difference in performance of the two similar type-same size engines could be due to the simple fact that the two engines are physically different. Factors such as differences in intake system design, valve timing, valve size, spark timing, *etc*. can contribute to these performance differences. This project is concerned with how close the fuel consumption and efficiency values of these two engines are at the common torque-speed indices.

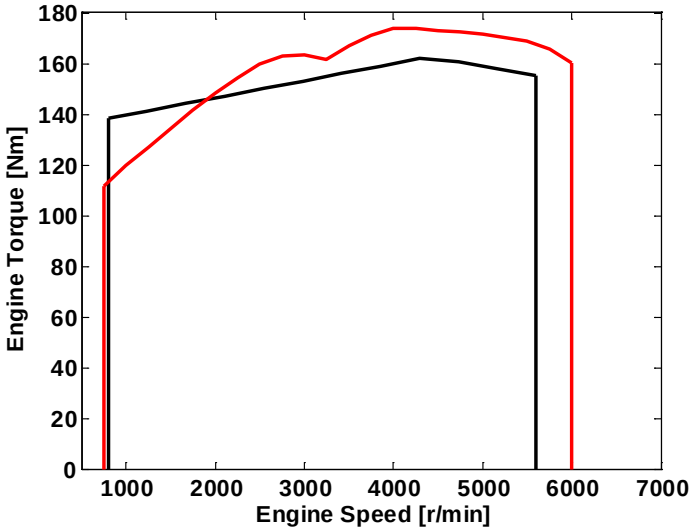

Figure 38: Maximum Torque-Speed Curves of 1.8 L NA-SI Engines (1&2)

Figure 38 shows the maximum torque curves of the two 1.8 L NA-SI engines. The red line in Figure 38 represents engine (2) and the black line represents engine (1). It can be seen that the region within the black lines contributes to most of the common region between the two engines. Hence, the fuel consumption and efficiency data for engine (2) was interpolated at the torque-speed indices of engine (1). Next, the fuel consumption and efficiency of the two engines at these same torque-speed points were compared.

The percent difference between the fuel consumption and efficiency at each of the common torque-speed indices was determined using Equation (4.1) and Equation (4.2) respectively. It would be ideal for most of these points to yield zero as two similar type-same size engines are expected to consume same fuel and be equally as efficient at the same operating torque and speed. Due to some of the possible differences mentioned earlier within these engines this is most likely not possible.

$$\Delta \dot{m} = \frac{\dot{m}_{actual1} - \dot{m}_{actual2}}{\dot{m}_{actual1}} \tag{4.1}$$

$$\Delta \eta = \frac{\eta_{actual1} - \eta_{actual2}}{\eta_{actual1}} \tag{4.2}$$

Figure 39 and Figure 40 represent the error between the fuel consumption and efficiency of the two similar type-same size engine respectively. The contours in

Figure 39 and Figure 40 represent how much error occurs at the respective torque and speed while the histograms in the Figures represent the how many points (y-axis) fall into each interval of the error (x-axis).

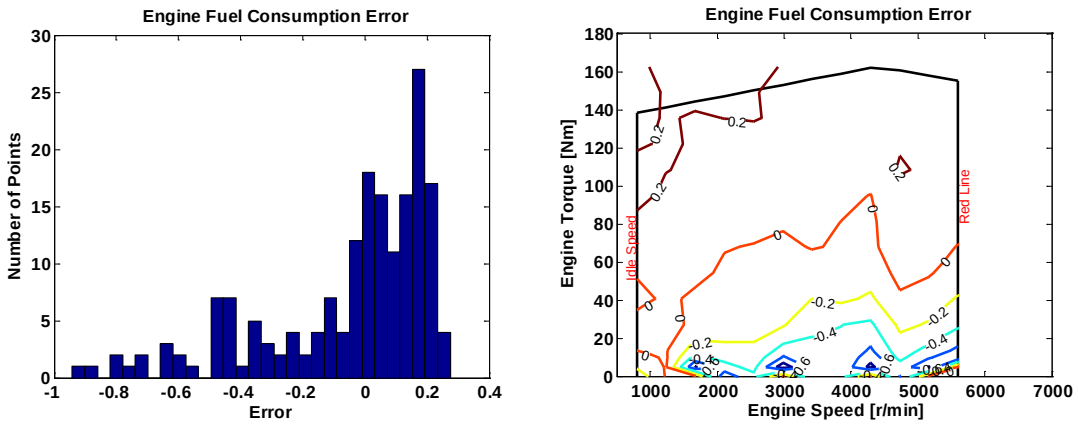

(a) (b)

Figure 39: 1.8 L Engine (1) vs. 1.8 L Engine(2) Fuel Consumption Comparison (a) Histogram, (b) Contour

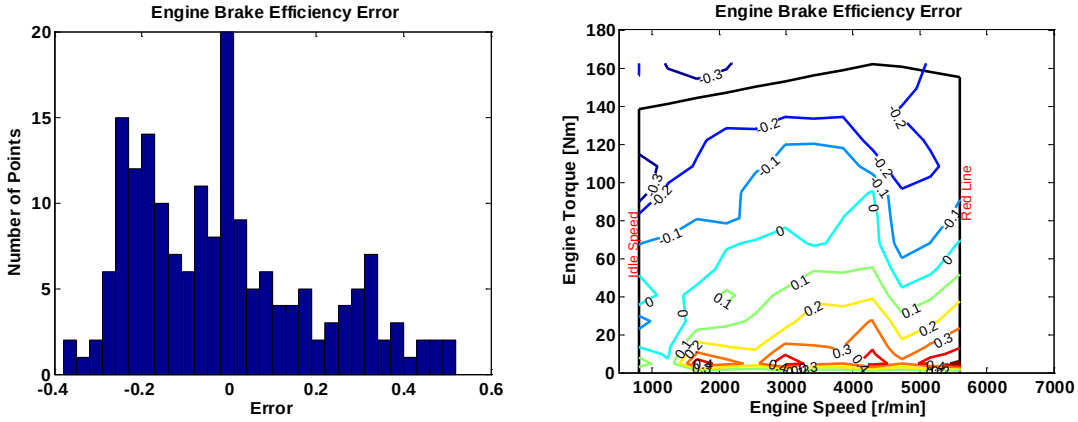

(a) (b)

Figure 40: 1.8 L Engine (1) vs. 1.8 L Engine(2) Efficiency Comparison (a) Histogram, (b) Contour

Looking at the both the contours in Figure 39 (b) and Figure 40 (b), it can be noticed that the very high errors (up to 49% for efficiency and up to 65% for fuel consumption) occurs in the low torque and high speed regions. The EcoCAR 3 vehicle, or rather any vehicle, rarely would operate in this low torque-high speed region, which does not make the high error in that region of the map a concern. Table 8 shows the mean and standard deviation

of all the fuel consumption and efficiency error points. Data shown in Table 8 represents that the means of both the fuel consumption and efficiency errors are less than 5 percent but, the standard deviations are on the higher side of 27 and 20 percent respectively.

Table 8: 1.8 L Engine (1) and 1.8 L Engine (2) Error Statistics

	Fuel Consumption Error	Efficiency Error
Mean	-0.05	-0.012
Standard Deviation ($\pm$)	.27	.20

4.2.2 Actual vs. Predicted Engines' Comparison

Moving forward, the predicted fuel consumption and efficiency data of the scaled 1.8 L engine is compared against the fuel consumption and efficiency data of the actual 1.8 L engine (1), the side by side comparison of which is shown in Figure 41. On the left side of Figure 41 (a & c), the fuel consumption and brake efficiency of 1.8 L engine (1) are shown and the same parameters for the predicted 1.8 L engine are on the right side (b &d). Table 9 lists the two engine's peak torque, peak power output, peak efficiency, and peak fuel consumption values and the indexed torque and speed where those points occur on their respective maps. Looking at Figure 41 and Table 9 it can be seen that the peak power and peak fuel consumption of both the engines occur at the same indexed torque and speed of the respective engines. The peak power output value and also the corresponding torque-speed indices where it occurs are different for both the engines but the peak fuel consumption is about the same.

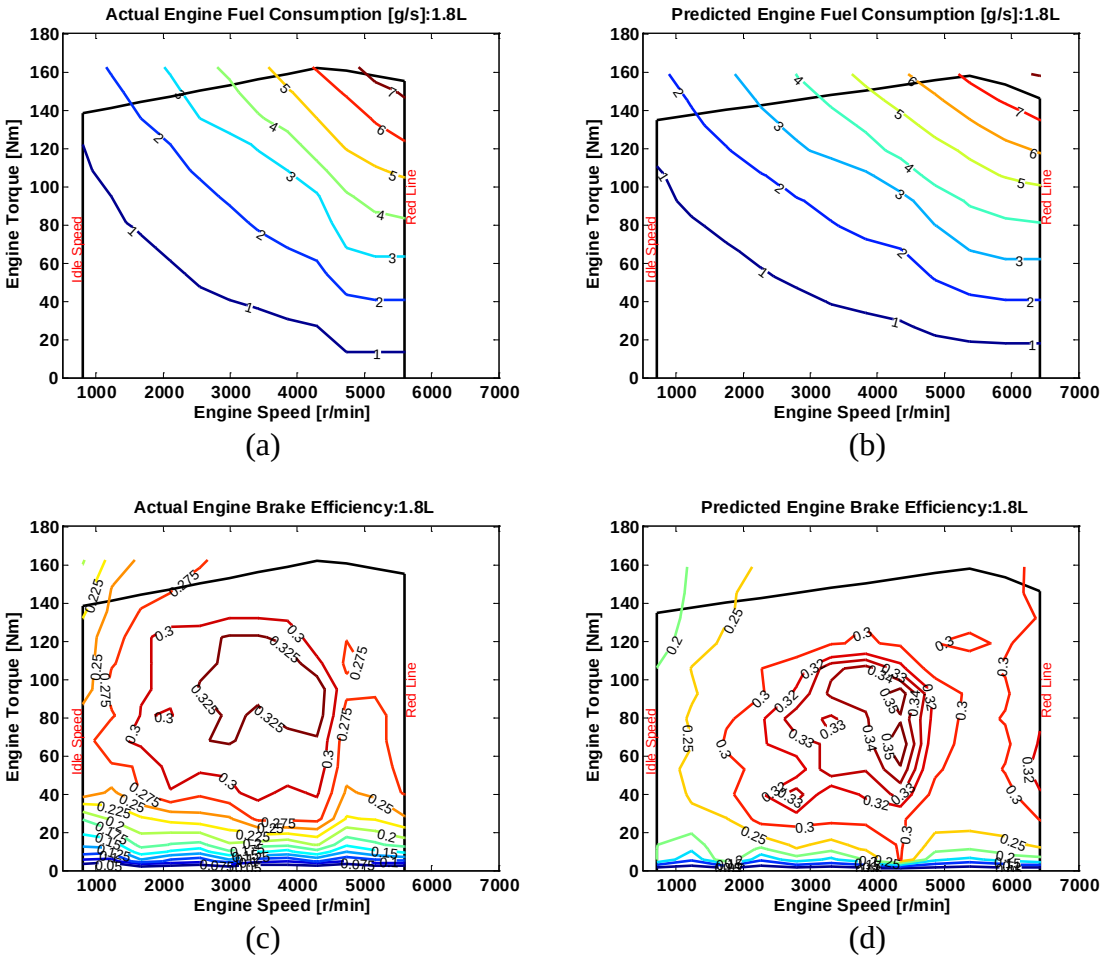

Figure 41: Actual vs. Predicted Engine's (a&b) Fuel Consumption and (c&d) Efficiency Comparison

Table 9: Actual vs. Predicted 1.8 L NA-SI Engines' Parameter Comparison

	NA 1.8 L SI engine (1)			NA 1.8 L SI engine (predicted)		
		Torque (Nm)	Speed (RPM)		Torque (Nm)	Speed (RPM)
Peak Torque (Nm)	162	162	4290	158	158	5384
Peak Power Output (kW)	90	155	5600	97.8	145.4	6421
Peak efficiency	33.94	108.5	3855	35.89	66.1	4345.7
Peak Fuel Consumption (g/s)	7.5	155	5600	7.45	145.4	6421

The peak torque of the predicted 1.8 L NA-SI engine is slightly lower than that of the actual 1.8 L engine and it occurs at a higher speed when compared to the speed where the peak torque occurs for the actual engine. The peak efficiency of the predicted engine is higher as compared to the actual engine. The predicted engine reaches its peak efficiency at a relatively lower torque and a higher speed when compared to the torque-speed index of the peak efficiency point for the actual engine. This difference in performance of the two similar type-same size engines could be due to the fact that the predicted engine was scaled using the data for a completely different 1.6 L NA-SI engine. The differences between the 1.6 L and the 1.8 L engine (1) can contribute to the performance difference between the predicted and actual 1.8 L engines. This project is concerned with how close the fuel consumption and efficiency values of two engines, predicted 1.8 L NA-SI and actual 1.8 L NA-SI (1), are at the common torque-speed indices. Figure 42 shows the maximum torque curves of the two 1.8 L NA-SI engines. The red line in Figure 42 represents the predicted 1.8 L NA-SI engine and the black line represents the actual 1.8 L NA-SI engine (1). It can be seen that the region within the black lines contributes to most of the common region between the two engines. Hence, the fuel consumption and efficiency data of the predicted 1.8 L NA-SI engine was interpolated at the torque-speed indices of actual engine (1).

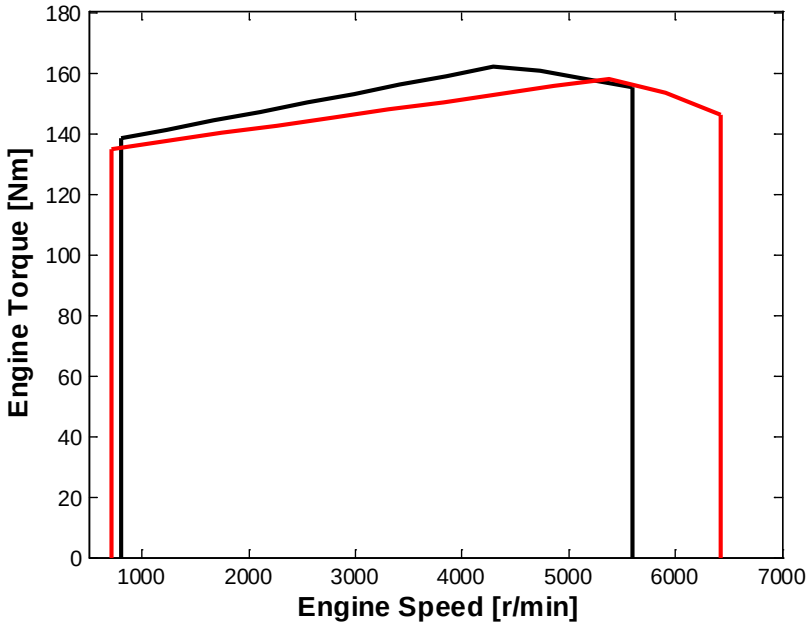

Figure 42: Maximum Torque-Speed Curves Comparison of Actual vs. Predicted 1.8 L NA-SI Engines

Next, the fuel consumption and efficiency of the two engines at these same torque-speed points were compared. The percent difference between the fuel consumption and efficiency at each of the common torque-speed indices was determined using Equation (4.3) and Equation (4.4) respectively. It would be ideal for most of these points to yield zero, as the predicted engine is expected to consume same fuel and be equally as efficient as the actual engine at the same operating torque and speed. But due to some of the possible differences mentioned earlier within the original 1.6 L engine and the actual 1.8 L engine (1), this is most likely not possible.

$$\Delta\dot{m} = \frac{\dot{m}_{predicted} - \dot{m}_{actual}}{\dot{m}_{actual}} \tag{4.3}$$

$$\Delta\eta = \frac{\eta_{predicted} - \eta_{actual}}{\eta_{actual}} \tag{4.4}$$

Figure 43 and Figure 44 represent the error between the fuel consumption and efficiency of the two similar type-same size engine. The contours in Figure 39 and Figure 40 represent how much error occurs at the respective torque and speed, while the histograms in the figures represent the how many points (y-axis) fall into each interval of the error (x-axis). Table 10 shows the mean and standard deviation of all the fuel consumption and efficiency error points. Looking at the both the contours in Figure 43 (b) and Figure 44 (b), it can be noticed that the very high errors (up to 67% for efficiency and up to 65% for fuel consumption) occurs in the low torque and high speed regions. As mentioned earlier, because a vehicle rarely would operate in this low torque-high speed region, high error in this region of the map is not of a concern. Data shown in Table 10 represents that the means of both the fuel consumption and efficiency errors are less than 9 percent but, the standard deviation are on the higher side of 17 and 20 percent respectively.

Finally, a comparison between the fuel consumption and efficiency error data, represented in 4.2.1 and 4.2.2 of actual vs. actual and actual vs. predicted engines' comparison is done. To contrast the difference the histograms of the fuel consumption and efficiency error data for both the comparisons done in this section are placed side by side as represented in Figure 45. On the left side of Figure 45 (a & c), the histograms for engine efficiency error and fuel consumption error obtained from predicted vs. actual engines' comparison are shown and the histograms for the same parameters for the actual vs. actual

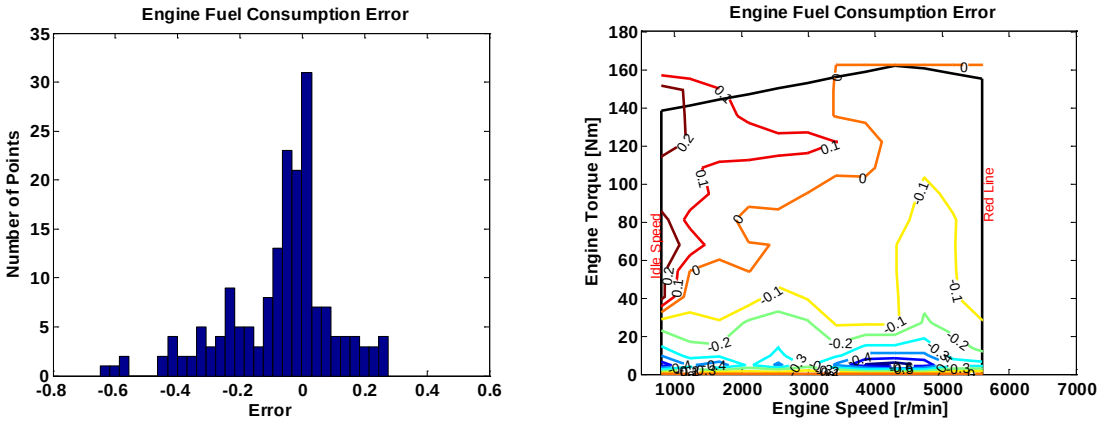

(a) (b)

Figure 43: Actual (1) vs. Predicted 1.8 L Engine Fuel Consumption Error (a) Histogram, (b) Contour

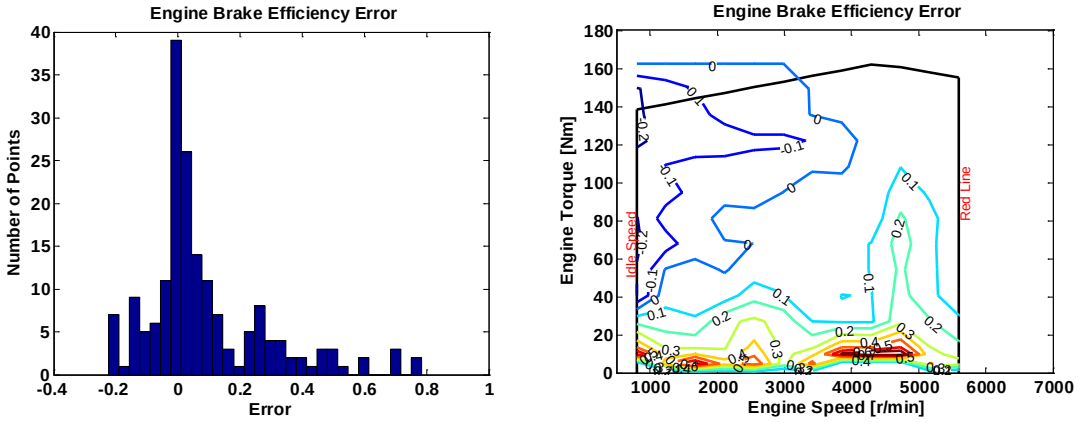

(a) (b)

Figure 44: Actual (1) vs. Predicted 1.8 L Engine Efficiency Error (a) Histogram, (b) Contour

Table 10: Actual 1.8 L Engine (1) and Predicted 1.8 L Engine Error Statistics

	Fuel consumption Error	**Efficiency Error**
Mean	-0.070976	0.088304
Standard Deviation(±)	.17	.20

engines' comparison are on the right side (b & d). Table 11 represents the means and standard deviations of both the fuel consumption and efficiency errors of both the comparisons.

Looking at Figure 45 it can be seen that the errors (fuel consumption and efficiency) obtained when the two actual engines were compared (b & d) are much more dispersed about the zero error as compared to the errors obtained from the predicted vs. actual engines' comparison. This could be the reason that the means of the errors for actual vs. actual comparison are lower than the means of the errors obtained from predicted vs. actual comparison, as can be seen in Table 11. The standard deviation for the errors obtained from prediction vs. actual comparison are lower for the fuel consumption and same for the efficiency as compared to the standard deviation for the errors obtained from actual vs. actual comparison. The mean and the standard deviation values of the error obtained from the 2 comparisons show that the engine scaling tool is scaling the engines accurately and can be used by the EcoCAR 3 team.

More simply put, the scaled version of the 1.6 L to 1.8 L engine is just as similar as one 1.8 L engine is to another 1.8 L engine. Given the goals of the high-level vehicle design tasks that this scaling tools will be used for, this accuracy is sufficient.

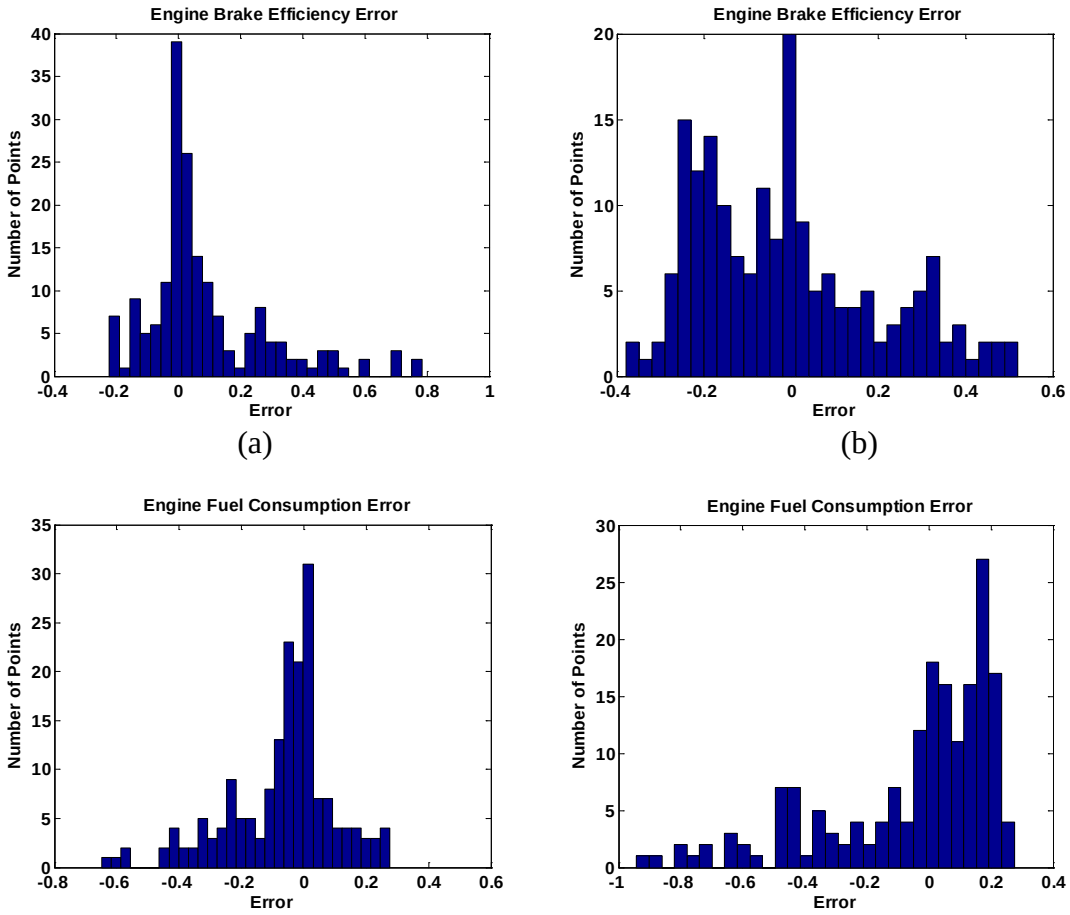

Figure 45: Predicted vs. Actual (a&c) and Actual vs. Actual (b&d) Efficiency and Fuel Consumption Error Histograms

Table 11: Actual vs. Actual and Predicted vs Actual Efficiency and Fuel Consumption Error Statics

		Fuel Consumption Error	Efficiency Error
Predicted vs. Actual Engines	**Mean**	-0.071	0.088
	Standard Deviation(±)	.17	.20
Actual vs. Actual Engines	**Mean**	-.05	-.012
	Standard Deviation(±)	.27	.20

4.3 Electric Machine Scaling

Unlike the engine scaling validation, to validate the EM scaling method adopted by this project, only one comparisons is done. This is due to the reason that not enough data was available to make the second comparison. The energy conversion data for existing brushless PM motors available to the EcoCAR 2 team through Parker-Hannifin were: the GVM210-100, which has a rotor of 100 mm stack length and the GVM210-150, which has a rotor of 150mm stack length, both with a common radius rotor. The rotor volumes for GVM210-100 and GVM210-150 are 1.4 L and 2.1 L respectively. This project scaled another 2.1 L PM motor, from the 1.4 L rotor EM, using the tool developed in this project as shown in Chapter 2:. The scaled 2.1 L rotor EM had the same physical parameters (rotor volume and rotor radius) as the already existing brushless PM motor with a 2.1 rotor. The predicted energy conversion efficiency data of the scaled EM with 2.1 L rotor is compared against the energy conversion efficiency data of the actual PM motor with 2.1 L rotor, both of which have the same physical parameters. Figure 36 shows all the data available and the dotted boxes around the boxes show the comparisons done for this project.

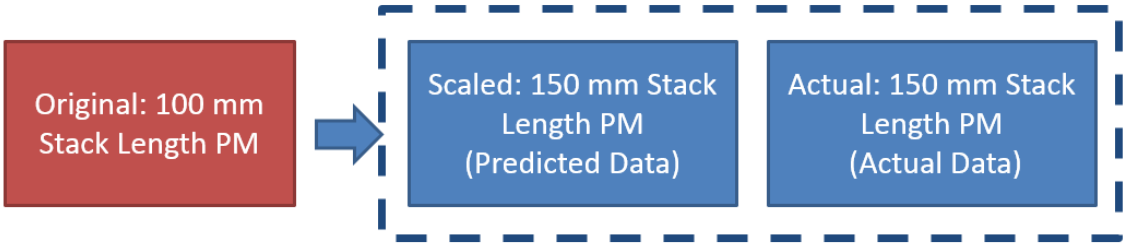

Figure 46: Electric Machine Comparisons

4.3.1 Actual vs. Predicted EM Comparison

The predicted energy conversion efficiency data of the scaled EM with a 2.1 L EM is compared against the energy conversion efficiency data of the actual EM with a 2.1 L EM, and the side by side comparison can be seen in Figure 47. On the left side of Figure 47 (a), energy conversion efficiency of the actual EM is shown and the efficiency map for the predicted EM is on the right side (b). Table 12 lists the two EM's peak torque, peak power output, peak efficiency, and stall continuous torque values as well as the indexed torque and speed where those points occur on their respective maps. Looking at Table 12 and Figure 47 it can be seen that the predicted motor with 2.1 L rotor has a lower power output, higher peak, and stall continuous torque but the same peak speed when compared to the actual EM with 2.1 L rotor. The same peak speed for both the EMs could be due to the same radius of the predicted and the actual motors' rotors. Peak energy conversion efficiencies of the two EMs is about the same but the corresponding torque-speed indices where it occurs are different for both the EMs. The actual EM reaches its peak efficiency at a higher torque and speed as compared to the predicted EM. The base speed, the speed that separates the constant torque and constant power region, of the two EM's is also different. The predicted motor has a base speed value of 4000 RPM compared to 5000 RPM of the actual EM. This difference in performance of the two similar type-same size EMs could be due to the differences between the original actual EM (brushless PM motor with a 1.4 L rotor), used to scale the predicted 2.1 L EM, and the actual EM with the 2.1 L rotor. Physical differences between the two motors or in the inverter calibration explain

these differences. This project is concerned with how close the energy conversion efficiency values of these two EMs are at the common torque-speed indices.

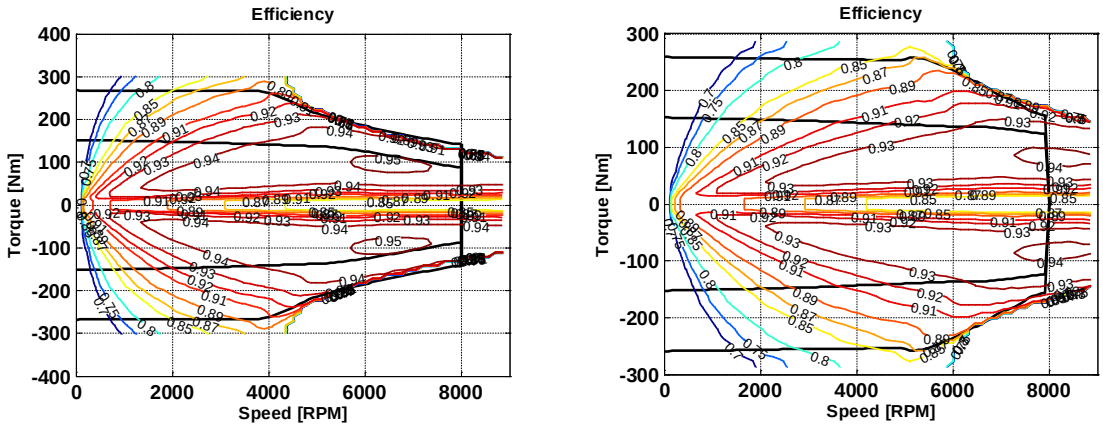

Figure 47: Actual (a) vs. Predicted (b) EM's Energy Conversion Efficiency Comparison

Table 12: Actual vs. Predicted PM Motors with 2.1 L Rotors' Parameter Comparison

	Actual brushless PM motor (2.1 L rotor)			Predicted brushless PM motor (2.1 L rotor)		
		Torque (Nm)	Speed (RPM)		Torque (Nm)	Speed (RPM)
Peak Torque (Nm)	260	260	0-5000	270	270	0-4000
Peak Power Output (kW)	135	260-156	5000-8000	115	270-143	4000-8000
Peak efficiency	94.1	86	7650	95	90.5	4345.7
Peak Stall Continuous Torque (Nm)	152	152	-	152	145.4	-

Figure 48 shows the maximum torque curves of the two brushless PM motors each with a 2.1 L rotor. The red line in Figure 42 represents the predicted EM's maximum torque and the black line represents the actual EM's maximum torque. It can be seen that the region within the red lines contributes to most of the common region between the two EM's

operating regions. Hence, the energy conversion efficiency data of the actual PM motor with a 2.1 L rotor was interpolated at the torque-speed indices of the predicted EM.

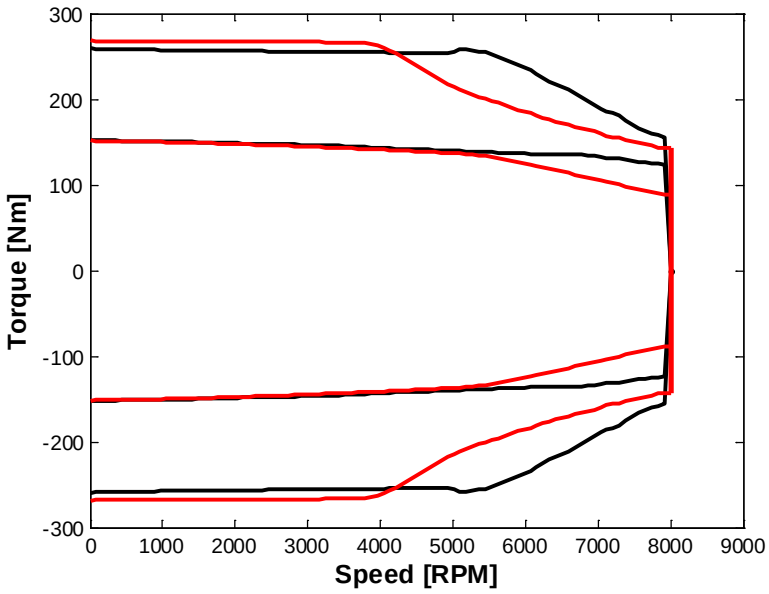

Figure 48: Maximum Torque-Speed Curves Comparison of Actual vs. Predicted EMs with 2.1 L Rotors

Moving further, the energy conversion efficiency of the two EMs at these same torque-speed points were compared. The percent difference between efficiency at each of the common torque-speed indices was determined using Equation (4.5). It would be ideal for most of these points to yield zero, as the predicted EM is expected be equally as efficient as the actual EM, with the same physical parameters, at the same operating torque and speed points. But due to some of the possible differences mentioned earlier between the original EM with a 1.4 L rotor and the actual EM with 2.1 L rotor this is most likely not possible.

$$\Delta\eta = \frac{\eta_{predicted} - \eta_{actual}}{\eta_{actual}} \tag{4.5}$$

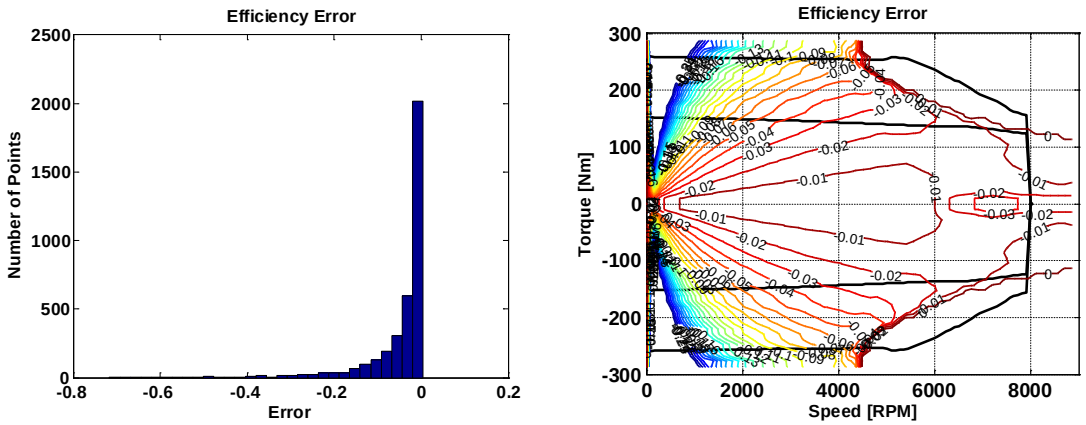

Figure 49: Actual vs. Predicted EMs with 2.1 L EMs' Fuel Efficiency Error (a) Histogram, (b) Contour

Figure 49 represents the percent difference between the efficiencies of the two (predicted vs. actual) similar type-same size EMs. The contour in and Figure 49 (b) represent how much percent-error occurs at the respective torque and speed, while the histograms in the figure represent the how many points (y-axis) fall into each interval of the error (x-axis). Table 13 shows the mean and standard deviation of all the efficiency error points seen in Figure 49.

Table 13: Actual and Predicted EMs with 2.1 L Rotor Efficiency Error Statistics

	Efficiency Error
Mean	-.0484
Standard Deviation($\pm$)	.08

Looking at the contour in Figure 49 (b), it can be noticed that low error occurs in the entire map. The highest error noticed are at the low speeds (under 400 RPM) and of the highest one being 17%. The error in this region of the map is not of a huge concern. Data shown in Table 13 represents that the mean efficiency errors are less than 5 percent and the standard deviation are 8 percent, which are statistically acceptable numbers. The mean and the standard deviation values obtain shows that the EM scaling tool is scaling the EMs accurately and can be used by the EcoCAR 3 team.

CHAPTER 5: CONCLUSION AND FUTURE WORK

The tools developed and validated for this project are capable of scaling engine and electric machine data with the desired accuracy. The engine scaling tool scales the fuel consumption data of a baseline engine to a different size engine, belonging to the same category. The EM scaling tool scales the power (consumption and output) of a baseline EM to a different size EM, belonging to the same category. Currently, the EcoCAR 3 team is using both the tools for HEV architecture design for the Chevrolet Camaro, which the team will be receiving in December 2015.

For further advancement of the tool, developed in this project, different engines and electric machines with various technologies can be scaled and the accuracy for scaling the different technologies will have to be examined. If the tools scale the performance aspects of the engine and EM with different engine and EM technology respectively, in an acceptable fashion, a library of engines and EMs could be further developed. This would help the EcoCAR team test any energy converter of different technology and size within EcoSIM and help the team understand how performance of an HEV varies with more degrees of freedom.

CHAPTER 6: BIBLIOGRAPHY

1. Global Industry Analysts, I. *Stringent Regulations for Curbing Greenhouse Gas Emissions Drives Demand for Emission Control Catalysts*. 2013; Available from: http://www.prweb.com/releases/emission_control_catalyst/autocatalysts_market/prweb11342846.htm.
2. Quality, E.O.o.T.a.A., *EPA and NHTSA Set Standards to Reduce Greenhouse Gases and Improve Fuel Economy for Model Years 2017-2025 Cars and Light Trucks.* August 2012(EPA-420-F-12-05): p. 1-10.
3. Research consortium of the Indiana, M.a.O.L.M.I.O., *Driving Workforce Change: Regional Impact and Implications of Auto Industry Transformation to a Green Economy*. 2013. p. 7-12.
4. Bovee, K., *Design of the Architecture and Supervisory Control Strategy for a Parallel-Series Plug-in*

Hybrid Electric Vehicle, in *Mechanical Engineering*. 2012, The Ohio State University.

5. Chan, C.C., *The State of the Art of Electric, Hybrid, and Fuel Cell Vehicles.* Proceedings of the IEEE, 2007. **95**(4): p. 704-718.
6. Chan, C.C., A. Bouscayrol, and K. Chen, *Electric, Hybrid, and Fuel-Cell Vehicles: Architectures and Modeling.* Vehicular Technology, IEEE Transactions on, 2010. **59**(2): p. 589-598.
7. Tate, E.D., M.O. Harpster, and P.J. Savagian, *The Electrification of the Automobile: From Conventional Hybrid, to Plug-in Hybrids, to Extended-Range*

Electric Vehicles. SAE Int. J. Passeng. Cars - Electron. Electr. Syst., 2008. **1**(1): p. 156-166.

8. Zeman, J., *et al*., *Modeling and Optimization of Plug-In Hybrid Electric Vehicle Fuel Economy*. 2012, SAE International.
9. Ehsani, M., G. Yimin, and J.M. Miller, *Hybrid Electric Vehicles: Architecture and Motor Drives.* Proceedings of the IEEE, 2007. **95**(4): p. 719-728.
10. Energy, U.S.D.o., *U.S. HEV Sales by Model*. April 2014: Alternative Fuels Data Center.
11. Rizzoni, G., L. Guzzella, and B.M. Baumann, *Unified modeling of hybrid electric vehicle drivetrains.* Mechatronics, IEEE/ASME Transactions on, 1999. **4**(3): p. 246-257.
12. Heywood, J.B., *Internal Combustion Engine Fundamentals*. 1988, New York: McGraw-Hill.
13. Woldring, D., T. Landenfeld, and M.J. Christie, *DI Boost: Application of a High Performance Gasoline Direct Injection Concept*. 2007, SAE International.
14. Ricardo, *A Study of Potential Effectiveness of Carbon Dioxide Reducing Vehicle Technologies*. 2008, U.S. Environmental Protection Agency.
15. Zeraoulia, M., M.E.H. Benbouzid, and D. Diallo, *Electric Motor Drive Selection Issues for HEV Propulsion Systems: A Comparative Study.* Vehicular Technology, IEEE Transactions on, 2006. **55**(6): p. 1756-1764.

16. Momoh, O.D. and M.O. Omoigui. *An overview of hybrid electric vehicle technology*. in *Vehicle Power and Propulsion Conference, 2009. VPPC '09. IEEE*. 2009.

17. Rahman, Z., M. Ehsani, and K.L. Butler, *An Investigation of Electric Motor Drive Characteristics for EV and HEV Propulsion Systems*. 2000, SAE International.

18. Gao, D.W., C. Mi, and A. Emadi, *Modeling and Simulation of Electric and Hybrid Vehicles.* Proceedings of the IEEE, 2007. **95**(4): p. 729-745.

19. D. Assanis, G.D., R. Fellini, Z. Filipi, J. Liedtke, N. Michelena, and D.R. P. Papalambros, D. Rosenbaum, A. Sales, M. Sasena, *An Optimization Approach to Hybrid Electric Propulsion*

System Design. 1999.

20. Pries, J. and H. Hofmann, *Magnetic and thermal scaling of electric machines.* International Journal of Vehicle Design, 2013. **61**(1): p. 219-232.